Available online at www.sciencedirect.com
SCIENCE DIRECT®
ELSEVIER
Earth-Science Reviews 74 (2006) 73–111
EARTH-SCIENCE REVIEWS
www.elsevier.com/locate/earscirev

The Somma–Vesuvius volcano (Southern Italy): Structure, dynamics and hazard evaluation

G. De Natale *, C. Troise, F. Pingue, G. Mastrolorenzo, L. Pappalardo

INGV-Osservatorio Vesuviano, Via Diocleziano, 328, 80124 Naples, Italy

Received 26 February 2003; accepted 18 August 2005

Abstract

We review the main results, with several new analyses, obtained in recent times about the structure, present dynamics and hazard evaluation at Somma–Vesuvius volcanic complex. We present a global review and interpretation of structural features, both at local and regional scale, constrained both by seismic and petrological data. The local structure of Somma–Vesuvius is reviewed in three depth ranges, shallow, intermediate and deep. The shallow velocity structure is inferred by the joint inversion of shot and local earthquake arrival time data. The main feature pointed out at shallow depth is a high velocity anomaly at the crater axis, extending down to about 5 km of depth. Such an anomaly, first observed at Vesuvius, seems to be common to many other volcanoes. It can be interpreted in terms of the presence of solidified residual magma in the shallow conduits, accumulated in last eruptive cycles. The local seismicity is strongly clustered around this anomaly, due to the focusing effect of the rigidity contrast. The seismic occurrence appears as a result of the superposition of a background level, mainly due to gravitational instability of the Vesuvius cone, and of intense activity episodes, which possibly reflect episodic internal activity. Two main zones of magma accumulation in the upper crust are evidenced by the joint interpretation of seismic and petrological data. The first one, located in the depth range 4–6 km, is mainly constrained by the crystallisation depth of phonolitic magmas which fed Plinian and sub-Plinian eruptions; the second one, around 11–15 km of depth, is mainly constrained by reflected–converted seismic waves, and in agreement with crystallization depths inferred for the moderate eruptions. The study of the deep structure, performed by regional tomography with teleseisms, further points out magma roots at higher depths (15–30 km). An additional result for the deep structure, studied at regional scale and very important for geodynamic interpretations of the Tyrrhenian volcanisms, has been the evidence for a subducting slab under the Apennines, in an area where previous models hypothesised a slab window.

New original studies of crystal growth (phenocrystals and microlites) on the eruptive products allow to infer typical times of magma rising from such reservoirs, which appear very low, on the order of minutes to tens of minutes. Static deformation at this volcano, in the last 30 yr, has been detected by the joint use of levelling, GPS and DIFSAR techniques. It indicates subsidence, very concentrated in the crater area and in a narrow strip all around the volcanic edifice, with maximum rates less than 0.01 m/yr. Static deformation in the crater area appears in agreement with the mechanism of gravitational instability generating local volcano-tectonic seismicity, while the peculiar pattern around the volcanic edifice is probably due to the combination of extensional stress and volcanic loading, generating a ring normal fault-like structure. While the key results about structure and dynamics help to define pre-eruptive scenarios, a new probabilistic procedure to combine volcanological data and computer simulations has been used, in this paper, to build hazard maps giving the probability, at each location in the area, to be hit by a pyroclastic flow or to

* Corresponding author. Tel.: +39 81 6108370; fax: +39 81 610 8371.
E-mail address: pino@ov.ingv.it (G. De Natale).

0012-8252/$ - see front matter
doi:10.1016/j.earscirev.2005.08.001

experience a destructive fall-out deposit. The review and new results of this work give then the first complete picture of the state of the art in our knowledge about Somma–Vesuvius volcano.

Keywords: volcano structure; volcano dynamics; volcanic hazard; Mount Vesuvius

1. Introduction

The knowledge of structural features and dynamics of the Somma–Vesuvius volcano has strongly increased in the last years. The main reason for such growing interest has been the consideration of the extremely high risk of the surrounding area, where about 700,000 people live within a radius of only 10 km from the main crater. Such consideration led many institutions and researchers to pay increasing attention to the study of this volcano. The TOMOVES (Gasparini et al., 1998) and BROADVES (De Gori et al., 2001) projects, in particular, gave a strong pulse to the structural studies, changing a lot our ideas about the internal structure of the volcano.

Although many papers, in the last years, have dealt with Somma–Vesuvius, and the most of them on structural features inferred from seismic tomography (Zollo et al., 1996a; De Natale et al., 1998, 2004a; De Gori et al., 2001; Auger et al., 2001; Di Stefano and Chiarabba, 2002) a detailed model aimed to synthesize all the key information towards the reconstruction of the volcanic structure, volcano dynamics and hazard for volcanological and civil defense purposes still does not exist. In fact, as for many other cases in Earth Sciences, geophysical and petrological–geochemical data are often presented as separate issues, with negligible overlapping and almost no attempt to merge together the different information towards a general interpretation. In the case of Somma–Vesuvius, on the contrary, a joint interpretation of different data set to give a coherent picture of the volcano behaviour and hazard is particularly important, giving the extreme risk associated to eruptions.

This paper is aimed to present the first, and most comprehensive interdisciplinary model for the structure, dynamics and eruptive hazard of Somma–Vesuvius.

The first part of the paper is devoted to a careful review of the recent results about the substructure of Somma–Vesuvius volcano, both from seismic analyses and from geochemical data. The main focus is given on the possible depth location of the main magma chambers.

The second part presents data and models about the volcano dynamics, including earthquakes, ground deformations and mechanisms of opening and rising of magma as inferred from rock texture analyses. The main goal of this section is to interpret the present dynamics and to possibly delineate the pre-eruptive phenomena of the next eruptions.

The third part of the paper presents new results on the hazard evaluation from eruption products, obtained using a new Bayesian procedure able to synthesise in large series of computer simulations all the information contained in the eruptive history of this volcano. The hazard evaluation obtained in this way is represented by probability maps for pyroclastic currents impact and fall-out accumulation.

All the obtained results are then discussed to give a consistent picture of the present level of knowledge of this volcano and its present dynamics and hazard, building guidelines for volcano monitoring and forecasting procedures. In addition, we show that a considerable part of the large body of information obtained for this volcano can be used as a guide for the interpretation of structure and dynamics of other similar strato-volcanoes in the world.

2. The sub-structure of Somma–Vesuvius

2.1. Seismic analyses

2.1.1. Shallow structure (0–5 km)

Our knowledge of the internal structure of Somma–Vesuvius has strongly increased in the last years. The shallow structure has been studied mainly by transmission travel–time tomography, using both the controlled sources represented by shots fired during the 1994 and 1996 active tomography experiments, and the local earthquake P and S waves (Zollo et al., 1996a,b; De Natale et al., 1998). The transmission tomography for the shallower structure has been also integrated by studies of reflected waves (Zollo et al., 1996b). The main findings, for the shallow structure, are linked to the observed difference between the central part of the volcano, with respect to the lateral one. The first and main evidence, in fact, is for a higher rigidity of the core of the volcano, along the crater axis, which exhibits a strong positive contrast of P and S velocity. The high velocity P wave anomaly has been the first feature well evidenced by the active soundings performed in 1994

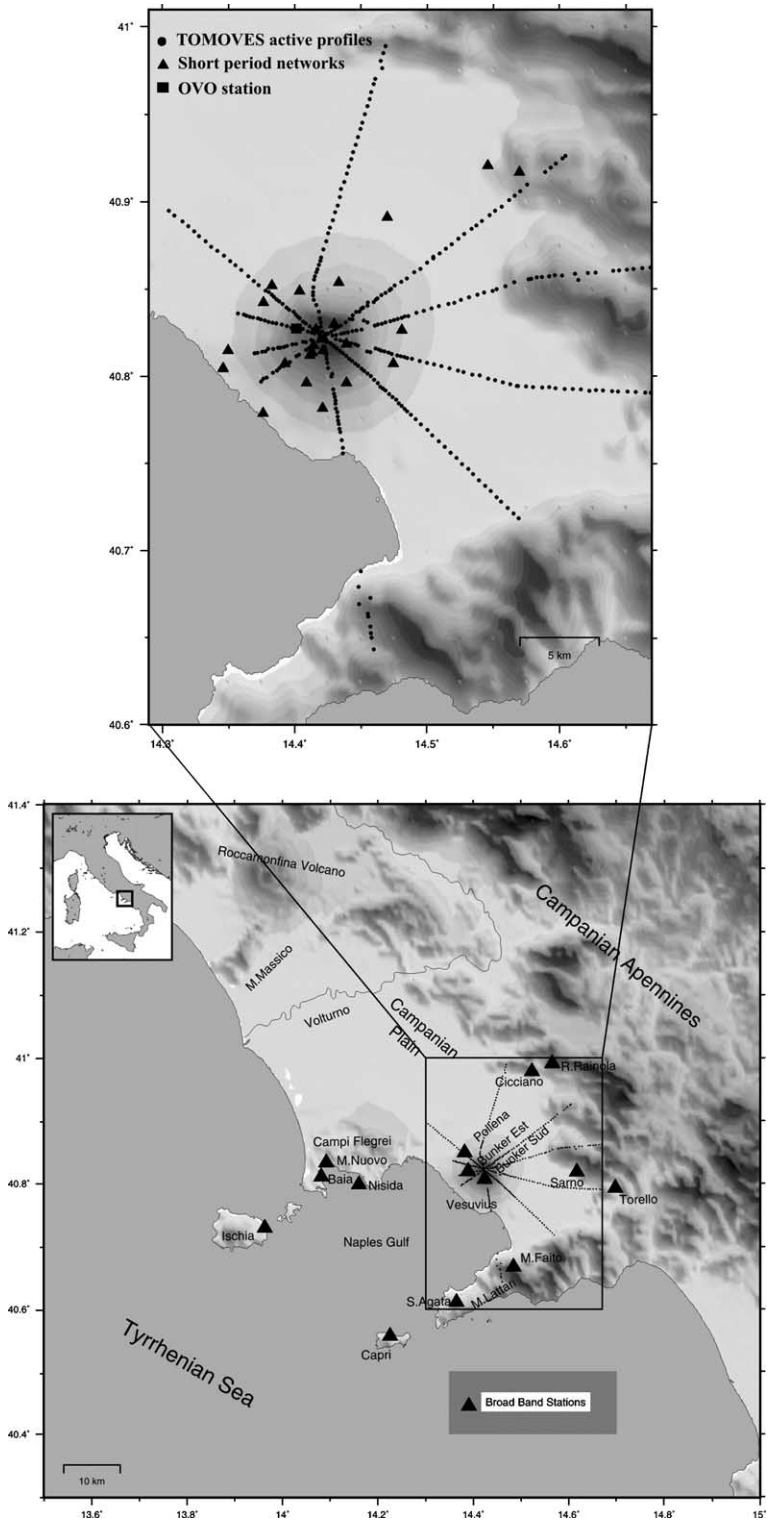

Fig. 1. Distribution of broad-band temporary arrays installed in the Somma–Vesuvius area during the BROADVES passive seismic experiment (1996–1997 and 1999). The inset indicates the short period seismic networks, both permanent and temporary, located in the Vesuvius area. Stations along profiles were installed during TOMOVES active seismic experiment (1994–1996) (after De Natale et al., 2001).

along a NW–SE profile crossing the Vesuvius crater (Zollo et al., 1996a,b). The 2D model obtained by the 1994 experiment was extended in 3D by De Natale et al. (1998), using the 2D model interpolated in 3D as initial guess and inverting P and S travel times from about 100 local earthquakes occurred at Somma–Vesuvius in the period 1987–1995, recorded by analogue and digital seismic stations of the Osservatorio Vesuviano. More recently, De Natale et al. (2004a) performed a detailed three-dimensional tomography using about 1000 local earthquakes, recorded from 1987 to the end of 1999, and 16 shots of the 1996 TOMOVES experiment. This study allowed the detailed reconstruction of the shallow structure under the Somma–Vesuvius volcano, from the crater top down to 5 km of depth.

Data for the tomographic inversions have been obtained from shots performed during the TOMOVES ('94 and '96) experiments and from local earthquakes recorded at Mt. Vesuvius by permanent and temporary seismic networks since 1987 (Fig. 1). In particular, P- and S-wave arrival times have been recorded by the permanent network of the Osservatorio Vesuviano (OV), in addition to data from temporary three-component digital stations installed since 1987 by the OV and other institutions (Istituto Nazionale di Geofisica and ETH-Zurich).

The 1970 earthquakes recorded during 1987–1998 have been located using Hypoinverse (Klein, 1989) and a 1D layered velocity model. For the tomographic inversion we selected only earthquakes having a minimum number of readings greater or equal to 8, and maximum r.m.s. residual less than 0.6 s. The upper threshold on the r.m.s. residual has been used to avoid including incorrect readings of arrival times in the data set.

The final data set used in the inversion consists of 3892 P-wave arrival times from 394 local earthquakes and 14 shots, recorded at 22 and 232 stations, respectively. A V_p/V_s model was computed using 1471 S–P times from local earthquakes. The inversion for V_p/V_s using S–P arrival times is preferred because of the lower number of S phases and the differences in reading uncertainties (Eberhart-Phillips and Reyners, 1997). A total of 886 V_p and V_p/V_s parameters are estimated at nodes of a

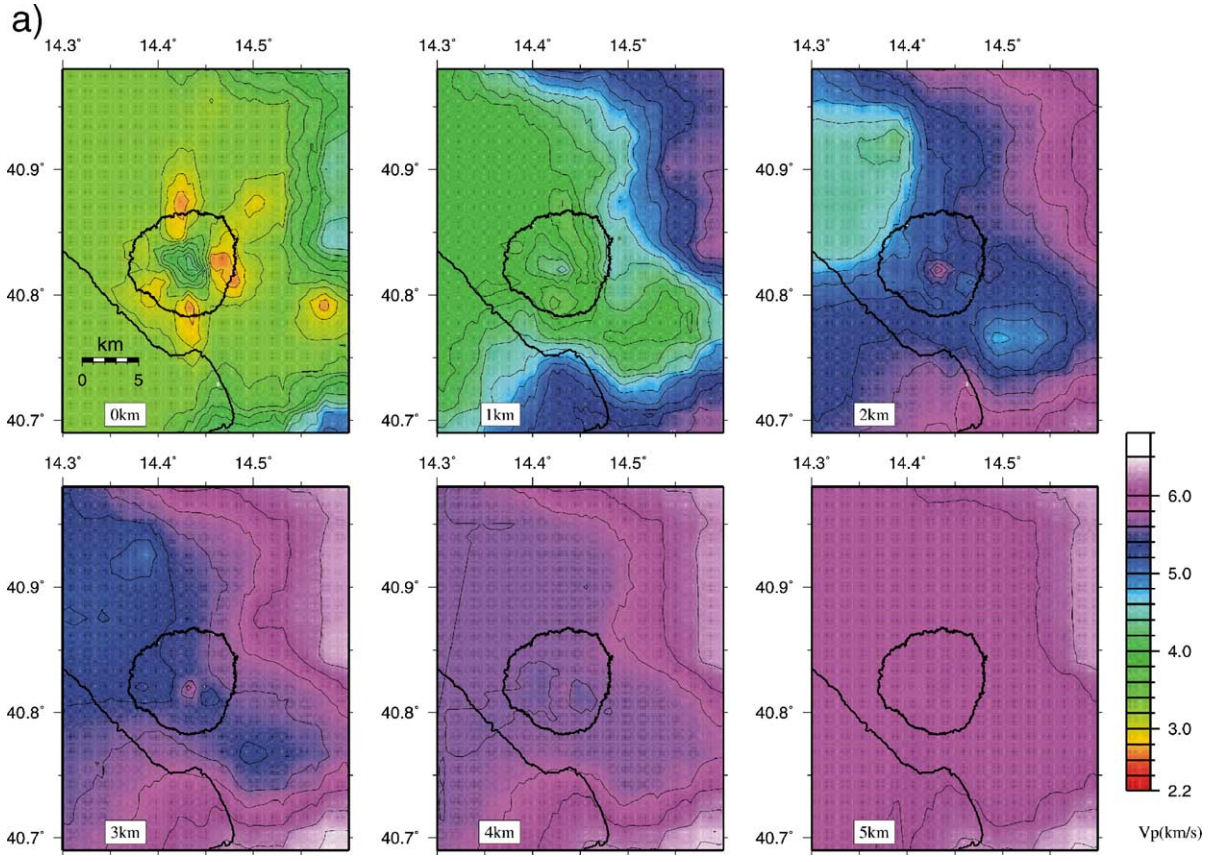

Fig. 2. Wave velocity shallow structure at Mt. Vesuvius as determined by De Natale et al. (2004a). (a) Map view of V_P velocity; (b) W–E and N–S depth sections of V_P velocity; (c) W–E and N–S depth sections of V_P/V_S velocity.

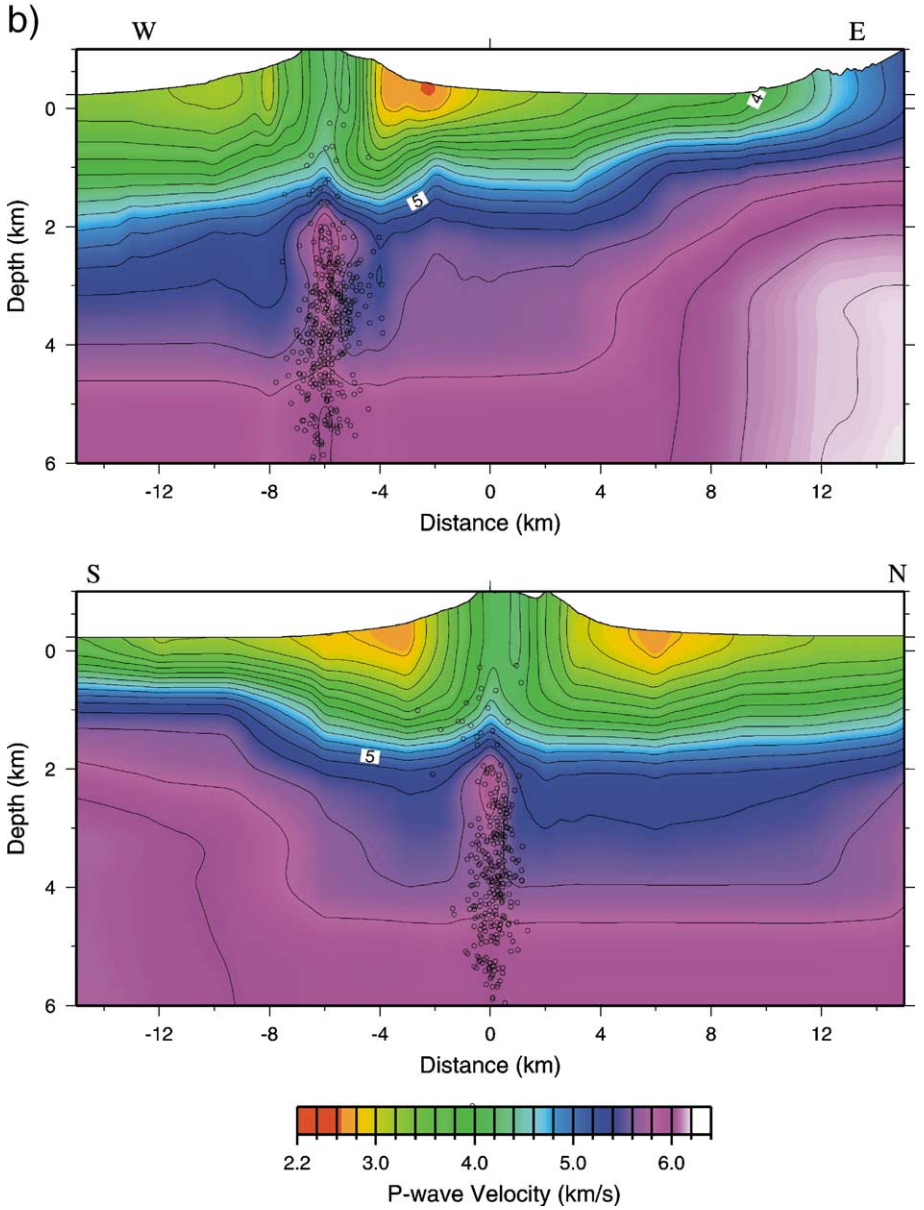

Fig. 2 (*continued*).

3D grid whose spacing has been chosen to optimize formal resolution and model definition, i.e., to identify the most detailed model resolvable with our data. We used, as starting model, a three-dimensional reference model in which V_p values at each node are set according to the tomographic model of Di Stefano and Chiarabba (2002), who inverted TOMOVES shot data with a robust adapted technique. The starting V_p/V_s value was set at 1.82. The final model, shown in Fig. 2, consists of 6 layers located at depths between 0 and 5 km, the deepest being used to fix the starting value for velocity. The nodes are spaced differently in each layer, varying from 1 km beneath the volcano to 3 km outside. In the very shallow structure (0–1 km) it is well evident the velocity contrast between the central part of the volcanic edifice and the lateral part, in particular the Somma rim. The central part appears characterised by a markedly high V_p velocity and higher magnetization (Fedi et al., 1998), whereas velocities along the slopes of Somma caldera appears considerably lower. At intermediate depths (2–3 km), the most evident anomaly in the volcanic edifice is still the central high velocity, which now

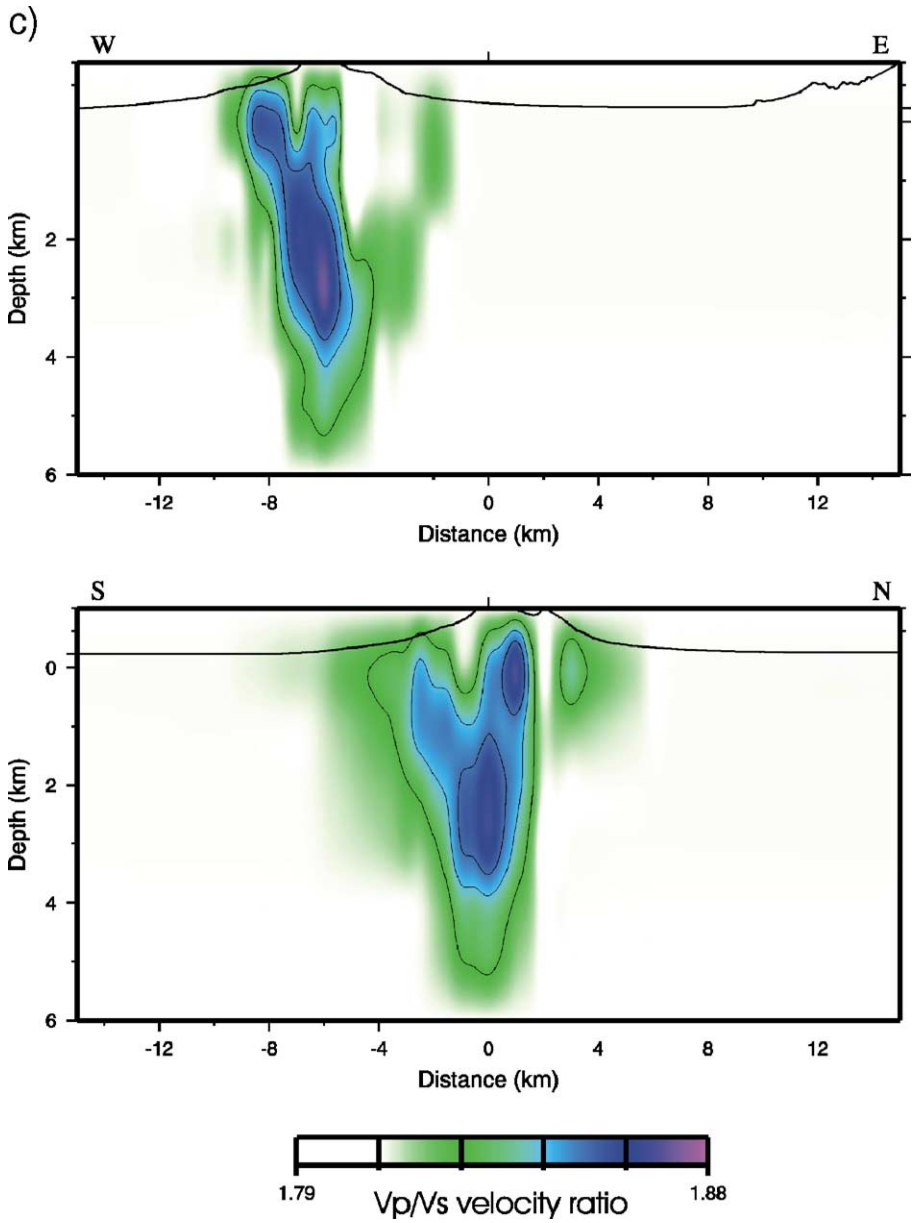

Fig. 2 (*continued*).

appears spread towards East. In the following, we discuss in details errors and resolution on these results.

For most of the data, the estimated reading uncertainties are about 0.05 s for P-onset on digital waveforms and around 0.1 s for S-wave arrivals.

Seismic tomography analysis is highly non linear, giving rise to well-known problems in estimating errors and resolution. Error estimates can only be obtained assuming linearity around local likelihood maxima for the parameters, and strongly depend on the regularization factors (in our case the amount of Levemberg–Marquardt damping). Resolution also depends critically on the amount of Levemberg–Marquardt damping and, due to the heterogeneity of the ray sampling, varies significantly throughout the sampled volume.

Ray sampling is the basic element determining the quality of a tomographic inversion. Fig. 3 shows the ray sampling for P and S waves in plan view (Fig. 3a) and cross sections (Fig. 3b). The cross sections show only ray paths sampling a thickness of ± 1 km from the section plane. It is evident how ray sampling is optimal at 3 km depth and along the shot profiles (for both of which

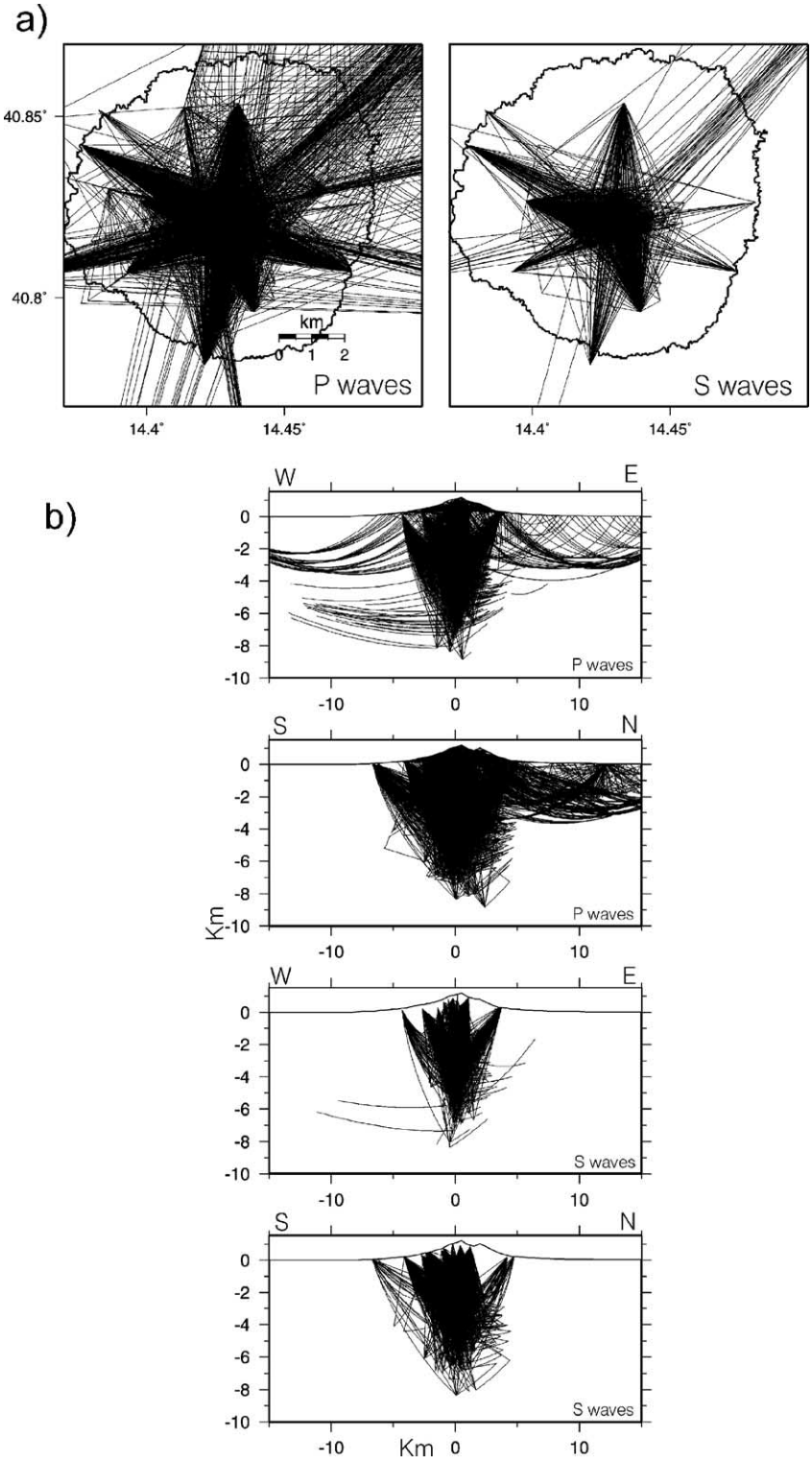

Fig. 3. Plots of ray sampling, both in a plane view (a) and in depth sections (b). (a) Plane view of both P (left) and S (right) rays, for all the depths. (b) W–E and S–N depth sections as shown in Fig. 5; each depth section shown has a thickness of ± 1 km.

active and passive source rays coexist). Below 4 km, ray sampling becomes progressively worse, and almost null below 7 km. Besides ray sampling, which can never be optimal across the whole volume, the main influence on the solution is given by applying the Levemberg–Marquardt damping, to handle the non-uniqueness.

Once the optimal value for the Levemberg–Marquardt damping is selected, on the basis of the best compromise between variance and resolution, covariance and resolution matrices can be computed, for yielding local estimates of errors and resolution. Using the selected damping factors for V_p and V_p/V_s, error estimates on the velocity parameters can be computed from the square root of the diagonal covariance matrix elements. Estimated errors on velocity values are in the range 0.01 to 0.02 km/s, depending on location, representing errors of less than a few percent of the observed variations. Such values are small, but, taken alone, do not say a lot about the solution, because small values of errors could be associated, via the chosen damping value, to very low resolution. In this work, we use a mostly innovative approach to compute resolution, that is able to quantify the actual size of the space in which a given level of resolution is contained. This is the most useful information to quantify the resolution of each parameter, i.e. the minimum size of the space in which each parameter is distinguishable from the others, and is generally lost in usual analyses showing only the diagonal elements of the resolution matrix (Menke, 1984). We used in fact a complete analysis of the resolution matrix to get the distribution of the resolution length, defined as the radius of the circle around each node that contains more than 68% of the resolution. To compute such a quantity we consider, for each grid point, the values of resolution at all the points. We sort the values in decreasing order, and take the value of the maximum distance, from each node, of the nodes included within 0.68 of the resolution sum. This gives an overestimate of the circular area in which 68% of resolution is enclosed. Fig. 4 shows that both V_p and V_p/V_s ratio has a generally good resolution length (between 0.5 and 3.0 km) for most of the Somma–Vesuvius edifice down to depths of 3 km. The central part of the volcanic edifice is still reasonably well resolved down to depths of 5 km. The

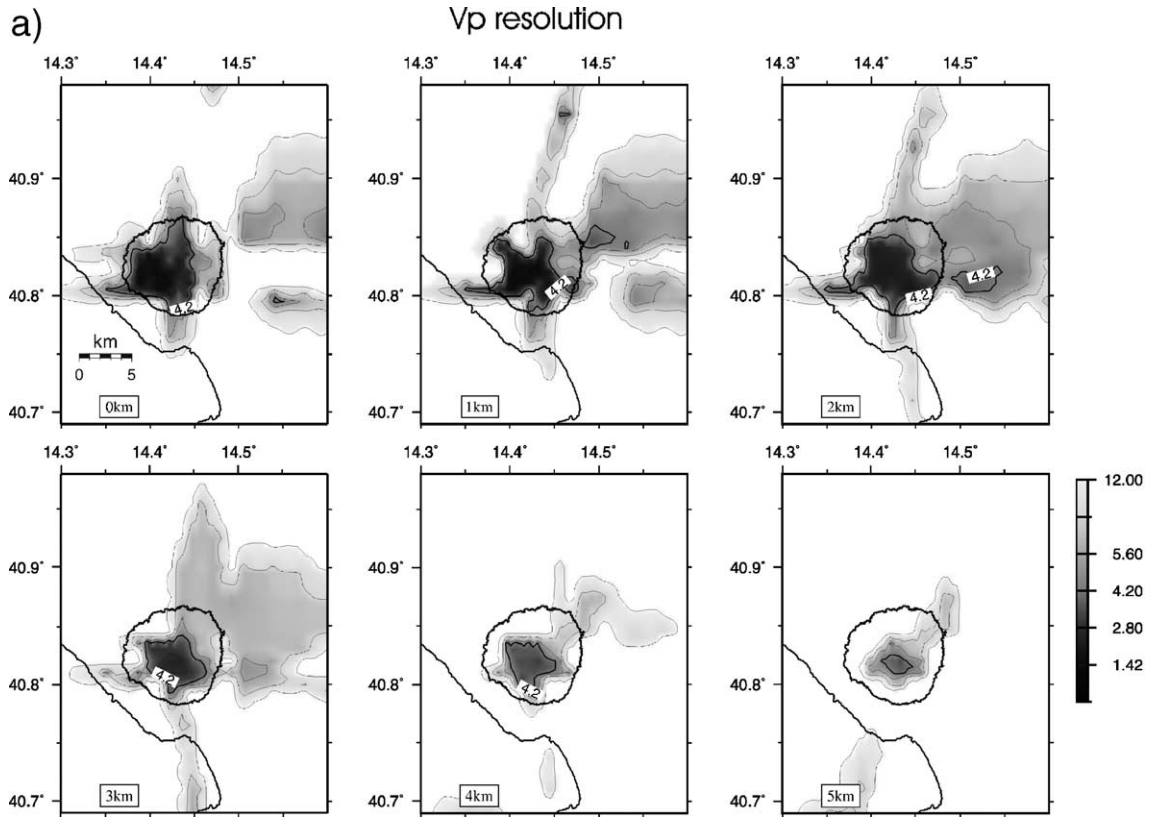

Fig. 4. Maps showing the length (in kilometers) of radius at each point of the velocity grid for V_p (a) and V_p/V_s (b). The radius is computed as the distance within which more than 68% of resolution at the given point is enclosed. Resolution at each point is computed in the linear approximation by the full resolution matrix.

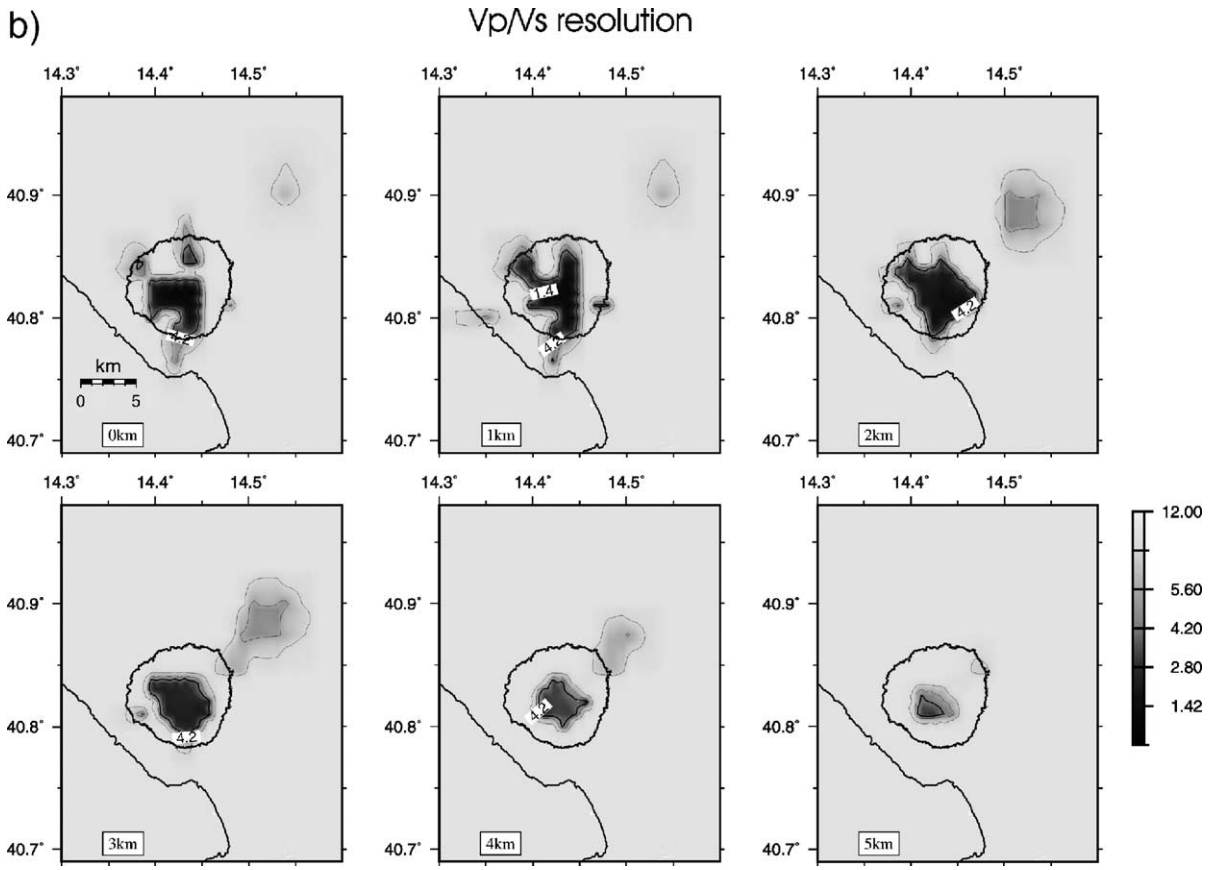

Fig. 4 (*continued*).

larger volcanic area is less resolved, with some sectors not resolved at all. These features of resolution are obviously related to the ray sampling, which is optimal for the surface structure because of cross-sampling of earthquake and shot rays, and, below 2–3 km, is only sampled by earthquakes which cover well only the central part of the volcanic edifice. Another source, although more indirect, of knowledge about the shallow structure of Somma–Vesuvius, comes from the direct observation of seismic clustering. Presti et al. (2004) showed that plots of seismic moment release, computed by a new probabilistic location algorithm, put in evidence two marked peaks, located, respectively, at about 2 and 5 km of depth (b.s.l.). These sharp peaks are ascribed to the presence of marked discontinuities in the shallow crust, which act like stress focusers. The shallowest peak can be reasonably ascribed to the average depth of carbonatic platform under the volcanic edifice, whereas the peak at 5–6 km, also discussed in De Natale et al. (2000), could represent the depth for the top of a shallow magma chamber, small enough to be hardly detectable by seismic tomography, located just below the depth termination of local seismicity.

2.1.2. Intermediate structure (5–15 km)

The intermediate structure of Somma–Vesuvius has been known, basically, from gravimetric studies (Berrino et al., 1998) and DSS surveys (Ferrucci et al., 1989). DSS surveys, however, have been mainly devoted to the deeper part, namely around the MOHO depth, and then left rather unknown the details of the structure in the range 10–20 km. The most evident discontinuity in this depth range, evidenced by both Bouguer anomalies and DSS studies, is associated to the crystalline basement (Mostardini and Merlini, 1986); In the last years, the studies of seismic tomography evidenced, at 8–12 km of depth, a marked discontinuity producing strong converted P–Sv waves (Zollo et al., 1996b; Auger et al., 2001). From detailed analyses of the converted wavefront, and from the relative amplitudes of the converted phases, such discontinuity has been interpreted as due to a sill-like magma chamber, located beneath the discontinuity. The precise size of such magma sill have been not yet unambiguously inferred, although Auger et al. (2001) postulate a size of 400 km^2 at least. The presence of a marked discontinuity at such a depth below the volcanic edifice has been recently

confirmed by P–Sv conversions from teleseisms, recorded by broad band three component stations (De Natale et al., 2001). Fig. 1 shows the location of broad-band stations operated in the Campania area in the framework of this experiments. Fig. 5 shows an example of broad-band seismogram of teleseismic event, recorded at the station Bunker Est. As noted by De Natale et al. (2001), such teleseismic record displays, at about 2 s from the first P arrival, clear converted S phases, more visible on the horizontal components. The depth that can be inferred by the observed S–P times, taking into account the structural tomographic model of the first 5 km of the crust, is in the range 11–15 km. Such depth agrees well with the results obtained by Zollo et al. (1996b), and is likely to mark the same intermediate discontinuity, which should represent a magma body. The proximity of such magma chamber to the depth of the crystalline basement as inferred from seismic and gravimetric studies (Corrado and Rapolla, 1981; Mostardini and Merlini, 1986; Berrino et al., 1998) suggests the emplacement of a magma sill, formed by a rising dyke stopped and horizontally channelled by the discontinuity between the limestone and the crystalline rocks.

This evidence is in agreement with the geochemical model of Pappalardo et al. (2002) that, on the basis of Sr–Nd isotopic variations in Campanian rocks, recognizes a magma reservoir in the eruptive basement. Recently, Natale et al. (in press) computed a V_s model from 0 to 30 km of depth by analysing the surface wave dispersion, finding a decrease of S wave velocity in the depth range 9–17 km which roughly include the depth ranges found by previous authors for the main magma chambers. This model is the only one computed for S waves below 5 km of depth.

2.1.3. Regional and deep structure (15–300 km)

The knowledge of the regional structure of the Campania region has also taken much benefit from recent studies, in particular those related to the BROADVES experiment, lasted from 1996 to 1999 (De Gori et al., 2001).

The data recorded in the framework of these experiments shed light both on structural features of Neapolitan volcanoes at intermediate-large depth, and on the large scale structure of this part of the Mediterranean area. We already mentioned the evidence of converted phases in the depth range 11–15 km below Somma–Vesuvius (De Natale et al., 2001). Broad-band seismic data have also enlightened the deeper regional structure, in conjunction with data from the Italian national seismic network. De Gori et al. (2001) have recently performed a travel time teleseismic tomography in the whole Campania–Apennine–Apulia region, merging broad-band data with analogue station recordings from the national network. Such a work benefited from the increased resolution due to the presence of BROADVES stations in the volcanic Campania area, to image the structure in the depth range 15–300 km under the Apennine, the Campanian volcanoes and the Apulia region with a considerably higher resolution. Fig. 6 shows a sketch map of velocity anomalies in the studied area.

In layer 2 (15–35 km depth), on the Tyrrhenian side, negative velocity perturbations are found beneath volcanic areas. In particular, a negative anomaly is imaged beneath the Vesuvius volcano, having an absolute magnitude of about 3%, well over the estimated uncertainty. Along the Tyrrhenian coast, a large area of low velocity (~−4.5%) is also found beneath the Roccamonfina volcano.

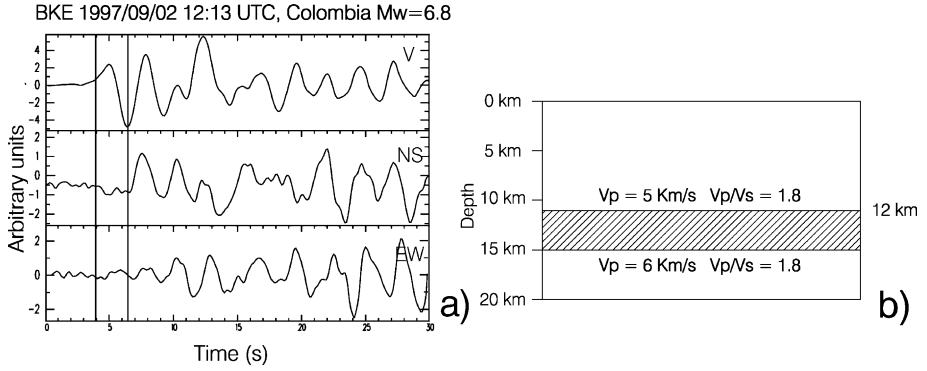

Fig. 5. a) Example of teleseism recorded by the broad band station Bunker Est, occurred on September 2, 1997. The upper trace is the vertical component, the intermediate is the horizontal component rotated in the direction station-earthquake, the bottom one is the horizontal, orthogonal one. Note the shift of about 2 s from the first pick P and the first pick of the horizontal, radial component. b) Scheme of the depth interval (shaded) of the conversion horizon inferred from the SV–P times at Bunker Est station. The position of the layer is a function of the assumed average V_p and V_p/V_s, as indicated on the scheme.

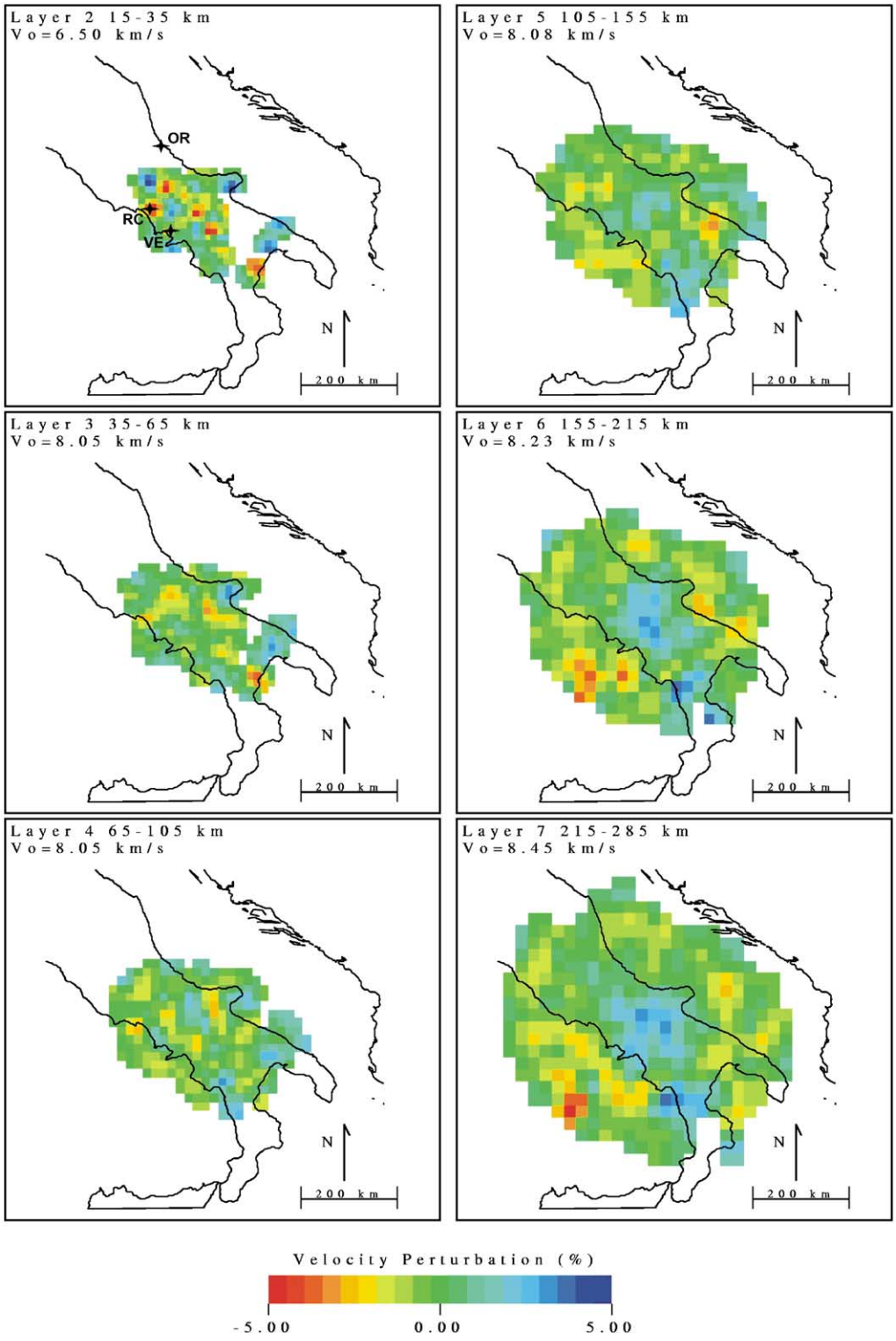

Fig. 6. Main results of teleseismic tomography. The figure shows P-wave velocity perturbations averaged on 4 position shifted grid, from layer 2 to layer 7. The reference velocities (V_0) are taken from IASP91 model. In the figure are also indicated the sites quoted in the text: Somma–Vesuvius (VE), Roccamonfina (RC) and Ortona (OR) sites (after De Gori et al., 2001).

High velocity regions (up to +3%) with a NW–SE trend are, on the contrary, observed beneath the Campanian Apennines.

A negative velocity perturbation, bordering the Campanian Apennines, characterizes the lower crust beneath southern Apennines and Bradanic foredeep and seems to be spatially related to the low velocity spot observed between the Calabria and Apulia regions.

In layer 3 (35–65 km depth), the main lateral heterogeneity displayed in layer 2 are still evident. The low velocity zone beneath the crust from Roccamonfina to the Adriatic coast appears less pronounced; the Vesuvius volcanic complex is characterized by an unperturbed upper mantle.

In layer 4 (65–105 km depth), three main high velocity regions are recovered, West of Gargano promontory, in central Apulia and in northern Calabria.

In layer 5 (105–155 km depth) we observe two clear positive anomalies, one SW of the Gargano promontory and the other beneath northern Calabria, separated by an unperturbed zone.

The pattern of the P wave velocity anomalies is also displayed in two vertical NE–SW sections (Fig. 7). Cross section AA′ displays a low velocity anomaly extending in the lower crust and in the uppermost mantle between the Tyrrhenian sea and the Adriatic coast. Weak velocity perturbations are found in the mantle beneath the belt with a relatively small high

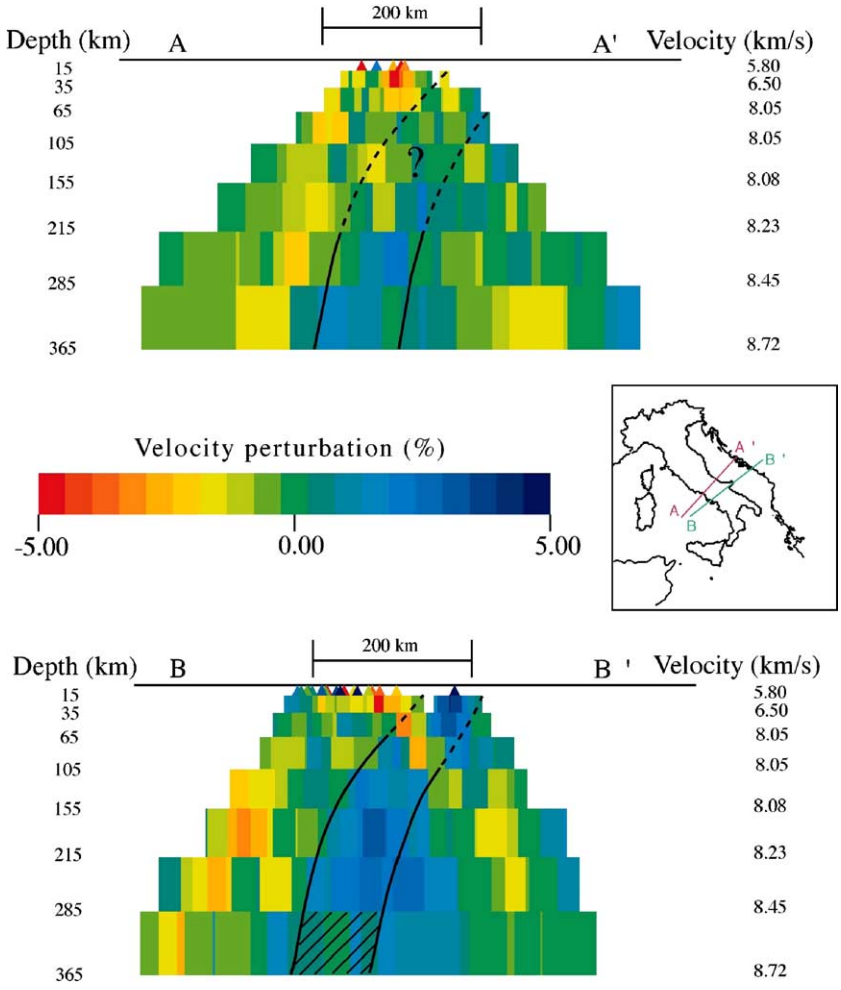

Fig. 7. Vertical sections through the velocity model along two profiles perpendicular to the Apennine chain. In the profile AA', an high velocity anomaly is detected below 200 km, which could correspond to a deep part of a subducting slab, whose prolongation is indicated by dashed lines. The section BB' displays an almost continuous high velocity body interpreted as the Adriatic lithosphere in subduction beneath the Apenninic belt (continuous line). The shaded part, below 285 km, corresponds to the anomaly evidenced by previous studies (Amato et al., 1993; Cimini and De Gori, 1997; Lucente et al., 1999). It is noteworthy that such previous studies had not good resolution in the shallow part, such to put in evidence the almost continuous anomalous body found with new data (after De Gori et al., 2001).

velocity anomaly dipping south-westward from 215 km depth.

The cross section BB′ (Fig. 7), extending from the Vesuvius volcano to the Gargano promontory, exhibits a very complex pattern of velocity anomalies. Beneath the Vesuvius volcano, a weak low velocity anomaly is found in the lower crust (−3%). An almost continuous high velocity body is reconstructed beneath the Apennines from 65 km down to 285 km depth. This feature can be related to the westward subduction of the Adriatic lithosphere, and was the first seismic evidence for a continuous subducting slab in this sector of the Italian peninsula, which had been hypothesized by petrological data (Peccerillo, 2001 and references therein). The recent paper by Panza et al. (2003) also contains seismological evidence supporting such an interpretation.

3. Geochemical and isotopical constraints on magma chamber location

Volcanological and petrological studies on Somma–Vesuvius products provide some further constraints about depth, dimension and physical proprieties of the magmatic system active during the history of the volcano.

The Somma–Vesuvius rocks are part of the potassic-rich Italian belt (Appleton, 1972) whose magmatism is related to the extensive tectonic phases developed during the opening of the Tyrrhenian sea. Two series of rocks have been recognized (Civetta and Santacroce, 1992): an older (>11.5 ka) KS (Appleton, 1972) ranging in composition from shoshonite to trachy-phonolite and a younger HKS ranging in composition from alkali-basalt to tephrite and phonolite. A scientific debate exists about the nature of the source of magmatism but most recent hypotheses converge versus a mantle source enriched by fluids or melts released by an undergoing oceanic slab (e.g. Peccerillo, 2001; Piochi et al., 2004 and reference therein).

Prolonged magma storage in the crust occurred at different time scale beneath the volcano as recorded by the degree of evolution of the erupted rocks. Major and trace elements and isotopic trends indicate that after their segregation from a mantle source, the primitive magma so derived, experienced complex mechanisms of replenishment and differentiation in magma reservoirs (e.g. Civetta et al., 1991; Civetta and Santacroce, 1992; Santacroce et al., 1993; Villemant et al., 1993; Cioni et al., 1995; Bertagnini et al., 1998; Landi et al., 1999; Del Moro et al., 2001; Civetta et al., 2004; Pappalardo et al., 2004).

Particularly, constrains on P–T conditions and volatiles concentrations of these reservoirs come from melts and fluid inclusions trapped in phenocrysts which grow in magma chambers. FTIR (Fourier transform infrared spectroscopy) analyses on inclusions in phenocrysts (e.g. Belkin et al., 1985; Belkin and De Vivo, 1993; Marianelli et al., 1999; Lima et al., 2003; Fulignati et al., 2004) indicate two different crystallization depths localized at 4 km and >11 km, respectively.

Following Pappalardo et al., 2004, the shallower chamber, always located within the carbonatic platform (e.g. Barberi and Leoni, 1980; Fulignati et al., 1998; Del Moro et al., 2001), supplied the Plinian and sub-Plinian eruptions that extruded the most evolved magmas at temperature of about 850–900 °C and volatile contents of about 2.5–6.0 wt.% (e.g. Cioni, 2000). In contrast, the deeper reservoirs fed the inter-Plinian volcanic activity, such as that between 1631–1944 AD, erupting the least evolved magmas at temperature of about 1150 °C and volatile content of about 3 wt.% (e.g. Marianelli et al., 1999; Fulignati et al., 2004).

A correlation exists between isotopical features of Vesuvius magmas and their crystallization depth. This relationship, interpreted and quantitatively modeled as deriving from crustal contamination processes (Pappalardo et al., 2004), indicates that the condition and timing of magma storage in the crust is a major controlling factor of the eruptive activity at Somma–Vesuvius. Less radiogenic (0.70730) mafic crystals have equilibrium crystallization depth exceeding 10 km, while more radiogenic (0.7075–0.7077) sialic minerals have shallower equilibrium crystallization depth of about 5 km. This suggests that the magmas acquired higher Sr-ratios by a process occurred subsequently to their genesis, when sialic minerals crystallized at shallow depth, in the chamber or in the conduit. Being the magma storage at very shallow depth (likely in the upper conduit) irrelevant, evidence of high Sr-isotope values of leucite at such depths implies that the contamination processes may occur even in relatively short time.

The change of Sr-isotopic ratios through the last 300 yr suggests that after the 1631 AD sub-Plinian eruption and until the last 1944 AD eruption none significant shallower reservoir was developed in the upper crust. This shallower reservoir probably grows during the long period of quiescence preceding the sub-Plinian and Plinian eruptions, by the periodical recharge of less contaminated magmas rising from deeper storage zone. This shallow reservoir was partially or completely emptied during major explosive events. In contrast the recurrence of the lower isotopic imprints in the

products of most of the Somma–Vesuvius eruptions, suggests that the deep reservoir can be considered long-lived reservoir acting during the whole volcanic history and furnishing at least 300 km^3 (Civetta and Santacroce, 1992) of magmas. This reservoir should be largely widespread beneath the Campanian area because magma storage of 11–22 km has been detected by isotopic imprints of magmas from the Campi Flegrei and Procida volcanic rocks (e.g. Pappalardo et al., 2002; De Astis et al., 2004).

4. Dynamics of Somma–Vesuvius

4.1. Stress field and earthquake generation

After the last eruption, occurred in 1944, Somma–Vesuvius volcano has been, till now, in a quiescent stage. The most considerable geophysical signal in such a period has been the occurrence of a background seismic activity, with some hundreds of earthquakes per year, on average (Berrino et al., 1993). Superimposed to

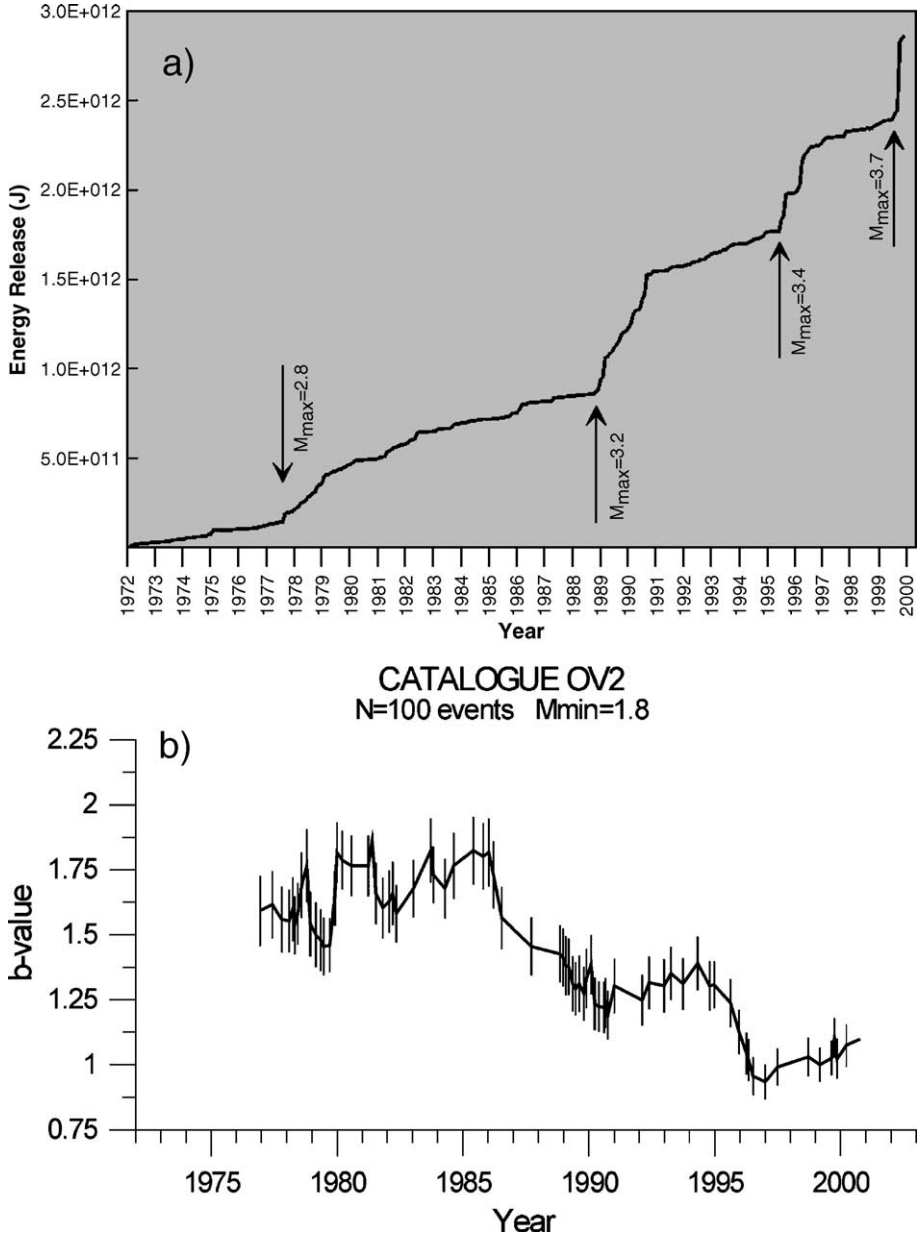

Fig. 8. (a) Monthly energy release curve in the period 1972–2000, computed from earthquake magnitudes (after De Natale et al. 2001). (b) Time variation of the *b* value of the Gutemberg–Richter relation computed by a maximum likelihood method (after De Natale et al., 2004b).

such background activity, are some episodes of higher seismicity, and higher magnitudes, reflecting a considerably higher strain rate. Fig. 8a shows the computed monthly energy release, as computed from magnitudes by the Kanamori (1977) formula, in the period 1972–2000. It is apparent that the episodes of increased seismicity level are characterised by progressively higher energy rates. The *b* value of the Gutemberg–Richter relation (Fig. 8b) also shows a marked variation during the analysed period, ranging from values around 2, at the starting periods to values less than 1 at present (De Natale et al., 2004b). The understanding of the mechanisms for local seismicity generation at Somma–Vesuvius requires to explain both the background level of activity and the occasional episodes of more intense swarms. It is likely that the occurrence of swarm episodes is related to some increased internal dynamics, while the mechanisms for background seismicity are far from being obvious. The occurrence of background seismicity at otherwise quiescent volcanoes is a rather common feature in central volcanoes (see for instance McNutt, 1996). Understanding the mechanism of generation of such seismicity is particularly important, in order to give insight into the dynamical state of the volcano in the last 50 yr. Earthquakes are recorded at Somma–Vesuvius since 1972, by analogue stations with Geotech S-13 and Mark L4-C 1 Hz sensors. The seismic surveillance network has been progressively improved since 1972, to get the actual network shown in Fig. 1. Some portable, digital stations have been added, in several periods, to the analog network, and they are also shown in Fig. 1. Fig. 9 reports the number of earthquakes per year as recorded at the station OVO, located at the site of the old building of the Osservatorio Vesuviano, built by the Bourbons kings in 1841. As it is clear, there is a background seismicity of some

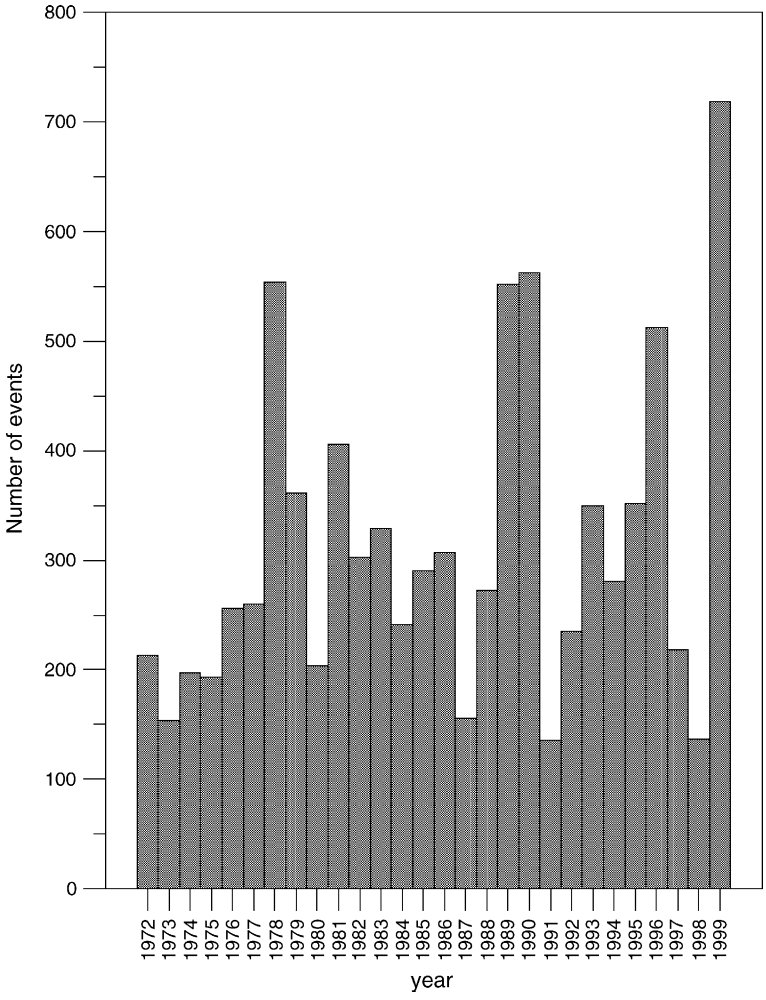

Fig. 9. Distribution of the number of earthquakes per year, as recorded at station OVO of Fig. 1, in the period 1972–2000.

hundreds of events per year, with occasional high seismicity periods, reaching peaks around one thousands of events per year. Fig. 8a also shows the times of occurrence of the events with magnitude over 3.0. Recorded local earthquakes range in magnitude from −0.5 to 3.6, the highest one recorded on October 9, 1999. As it is evident, periods with peaks in seismicity have also highest magnitude events. Such peaks occurred on 1989–1990, 1995–1996 (Capuano et al., 1999) and 1999–2000 (De Natale et al., 2004b).

The knowledge of the 3D velocity structure of the area, as inferred from tomography with shots and earthquakes, allowed to get accurate earthquake locations, as shown in Fig. 2. The earthquakes appear strongly clustered around the crater axis, within a radius of less than 1 km. Earthquake occurrence is practically coincident with the high rigidity anomaly evidenced by seismic tomography. A model for generation of background seismicity at Somma–Vesuvius and at similar central volcanoes has been recently proposed by De Natale et al. (2000). The basic feature of such a model is the high level of shear stress in the edifice, as due to the gravitational load of the volcano, strongly focused at the borders of the central rigidity anomaly. The model has been studied by a finite element, axial-symmetric scheme (Fig. 10). Fig. 11 (case I and II) reports the shear stress field, as due the gravitation load of the volcanic edifice, for different values of the density of the anomalous body. It can be compared with the corresponding field of case III, obtained for a homogeneous medium, to put in evidence the fundamental role played by the high rigidity anomaly in concentrating and amplifying shear stress around the crater axis. Fig. 11 (case IV) shows the shear stress produced, around the anomaly, by applying a uniform extensional stress at the borders of the finite element scheme. It simulates an external, regional stress change, in this case isotropic, which is converted, with an about 10% efficiency, in shear stress around the anomaly. Finally, Fig. 12 shows the maximum shear at depth as inferred from the model (broken line), as compared with critical thresholds for different kinds of mechanisms determined observationally, and reported by Hill (1992). The inferred depths of maximum shear stress compare very well with peaks in observed earthquake distribution (Fig. 12). The proposed model is then able to explain the main features of the local seismicity in terms of small stress perturbations acting on a gravitationally stressed structure, with shear stress strongly concentrated along the high rigidity axial anomaly.

The relation of the stress field with focal mechanisms and source parameter estimates seems rather complex, looking at the published literature on focal mechanism and source parameter estimates (Vilardo et al., 1996; Capuano et al., 1999; Auger et al., 2001; De Natale et al., 2004b; Del Pezzo et al., 2004). Computed focal mechanisms, in fact, show a large variety of mechanism types, although normal faulting seems to be dominant for larger magnitude events (Vilardo et al., 1996; Capuano et al., 1999; Del Pezzo et al., 2004). Furthermore, De Natale et al. (2004b), using an algorithm for waveform inversion, inferred a considerable isotropic component in several larger magnitude earthquakes, thus calling for an explosive component in the source mechanism, perhaps due to the contribution of an aquifer system in critical conditions. Source parameter estimates from seismic wave spectra show a marked constancy of the corner frequency, over all the range of seismic moments (Capuano et al., 1999; Del Pezzo et al., 2004). This feature has been interpreted both in terms of changing stress drop (Del Pezzo et al., 2004), and of a generalised strong site effect, which masks the real corner frequency particularly for larger earthquakes (Capuano et al., 1999).

We note that the De Natale et al. (2000) model would predict a dominant normal faulting mechanism, although within a large variability due to the small-scale heterogeneity of the more stressed surfaces with the highest rigidity gradients.

4.2. Surface static deformations from InSar, levellings and GPS data

Static ground deformation monitoring at Somma–Vesuvius is obtained by several geodetic systems, including levelling lines, continuous and periodic GPS networks, EDM, tiltmeters. In particular, a well developed system of levelling lines has been operating since 1970, and progressively enlarged until the actual size (more than 200 km of length, with reference benchmarks on the limestones of the Sorrento Peninsula, see Fig. 13). In the last decade, a well developed network of GPS benchmarks for periodic measurements has been installed, with denser sampling of the volcanic centers (Somma–Vesuvius, Campi Flegrei and Ischia) and global coverage of the whole volcanic–tectonic Campanian area (from the volcanic coast to the main tectonic domains of Apennines, see Fig. 13). In addition to permanent monitoring data, InSAR images in the period 1992–2000 have been processed to give a complete picture of the on–going deformation at Somma–Vesuvius (Lanari et al., 2002).

An overall view of the recent deformations detected by the different systems is shown in the maps of Fig.

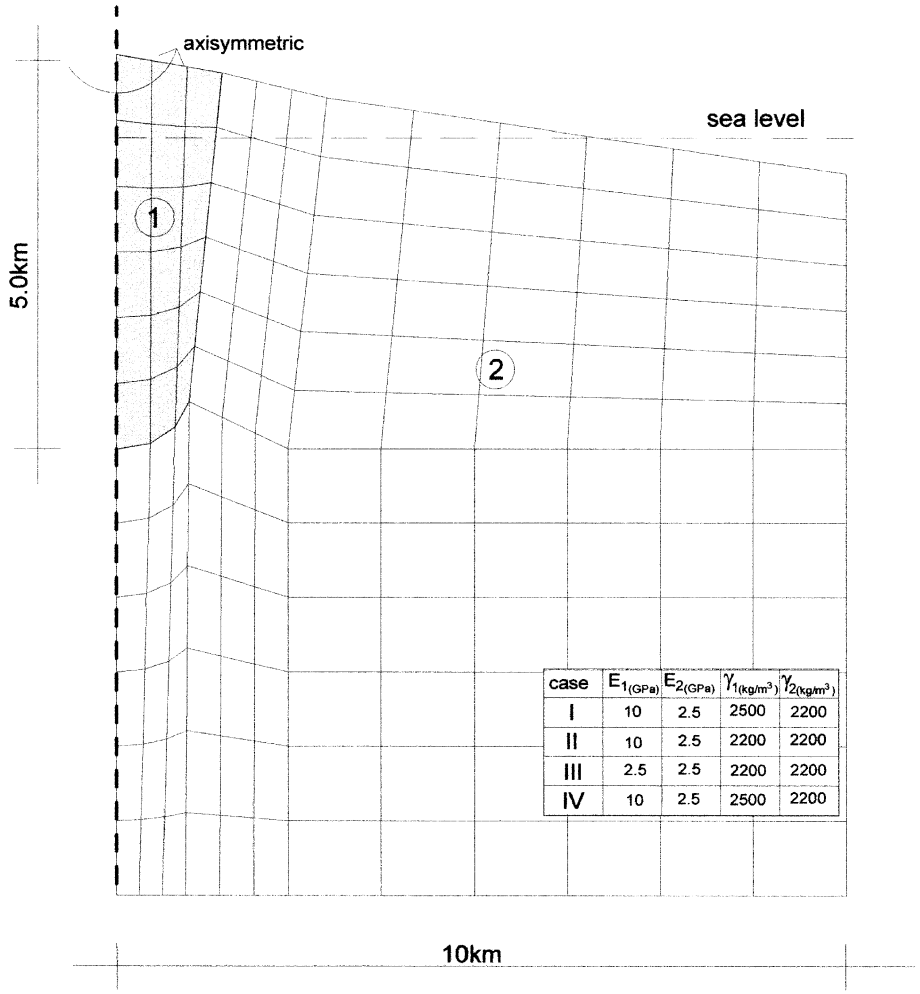

Fig. 10. 3D axial-symmetric mesh used for finite element computations of stress in the volcanic edifice. Roman numbers in the lower box indicate different computations, using the indicated set of Young moduli E and densities γ in the zones 1 and 2. The value of the Poisson ratio is fixed to 0.3 for all the runs. Also indicated is the reference system in polar coordinates (r, θ, z) (after De Natale et al., 2000).

14, relative to the time interval 06/1992–09/2000. The main color map shows the results obtained by processing InSAR data by an accurate unwrapping technique involving the analysis of 40 subsequent images covering the quoted period. In addition, the deformation time-series obtained by precise leveling at some selected zones are presented (see plots in Fig. 14 relative to the marked areas A, B, C, D, E) showing the temporal evolution of the displacements affecting these zones.

Two well-defined zones of subsidence are evidenced in the maps of Fig. 14. The first one is the central cone, the Vesuvius properly said, wherein reliable measurements are typically available in correspondence of lava structures where the coherence of the interferometric signal is preserved. Another zone of subsidence is represented by a narrow strip that extends, although not fully continuously, around the volcano at about 9–10 km of distance from the crater. At both the areas, subsidence appears to be rather continuous in the last 10 yr (see the time-series in plots (A)–(E) of Fig. 14) and characterized by an average rate in the range 0.3–0.8 cm/yr with a maximum cumulative subsidence in the range of 5–7 cm. Such subsidence pattern is unusual and hardly interpretable in terms of any meaningful volcanic source; however, it is interesting to note that both the subsiding zones lie at the contact between different rock lithologies. In the case of the central cone, subsidence would occur at the contact between the rocks of the younger Vesuvius activity and the older Somma structure; the external subsidence occurs at the contact between volcanic and non-volcanic rocks. Non-volcanic basement rocks, curved by the weight of the superimposed volcanic edifice, are mostly represented

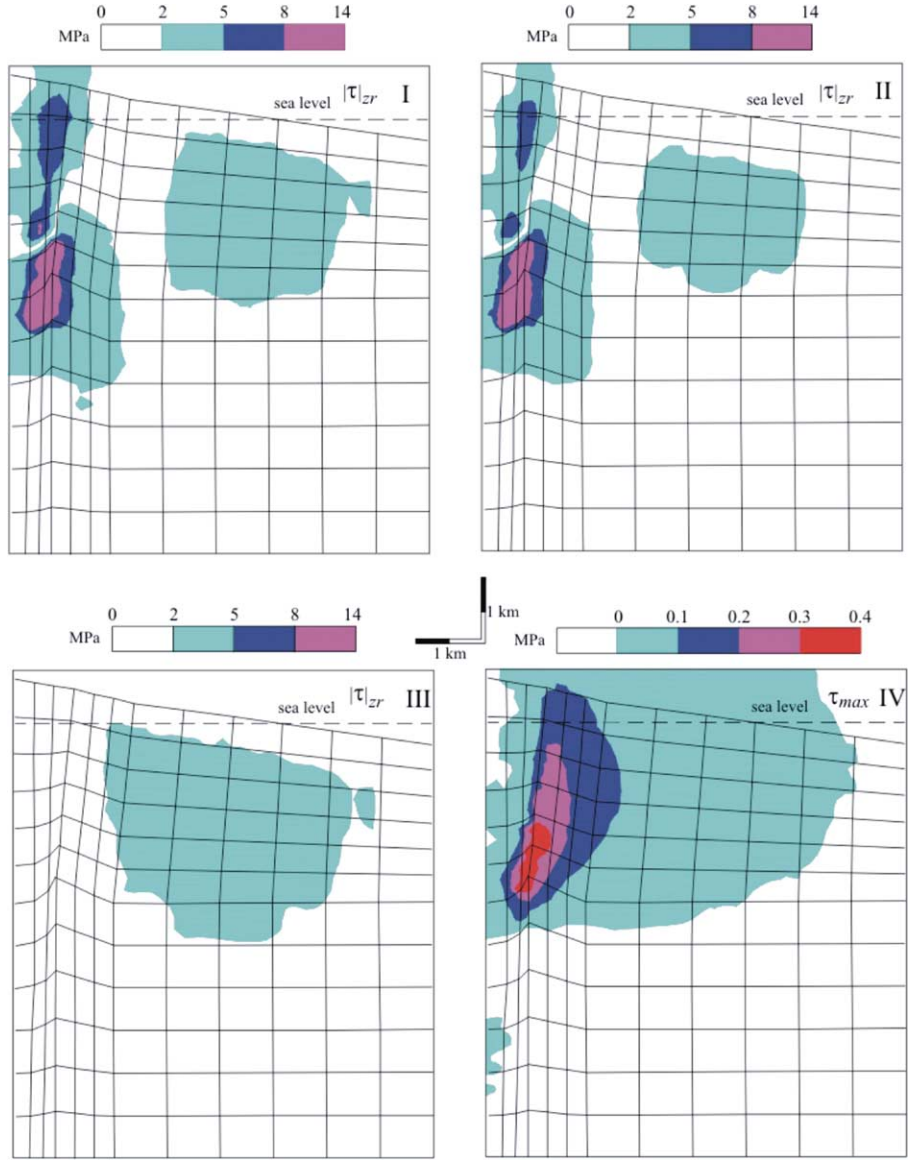

Fig. 11. Computed shear stresses for the four cases shown in Fig. 10. Case I and II show the results for shear stress in presence of the high rigidity axial anomaly, with and without density contrast. Case III shows what happens if the central high rigidity anomaly is absent. Case IV is for an applied homogeneous extension of 5 MPa at the lateral borders, simulating a regional stress. In this case, the shear stress shown is the maximum on the plane perpendicular to (r, z) (after De Natale et al., 2000).

by the carbonates of the Apennines and the Sorrento Peninsula, except in the W–NW sector, where they involve the basement rocks of the easternmost border of the Acerra basin.

The subsidence of the crater agrees well with our model for local seismicity being essentially driven by gravitational stress concentrated around the central high rigidity anomaly. In fact, subsidence would represent the surface expression of the gravitational instability of the central part of the volcano, causing also the seismicity.

The ring subsidence zone around the volcanic edifice would reflect, in the model proposed by Lanari et al. (2002), the slip along the contact between volcanic and non-volcanic rocks, induced by the joint effect of the tensional regional stress regime and the volcano loading. Since the contact surfaces between volcanic and external rocks have a low angle dip, the resulting movement under tensional stress is similar to a ring, low angle normal fault, which produces a subsiding ring stripe in the hanging wall, with almost no uplift on the foot wall (see Fig. 15).

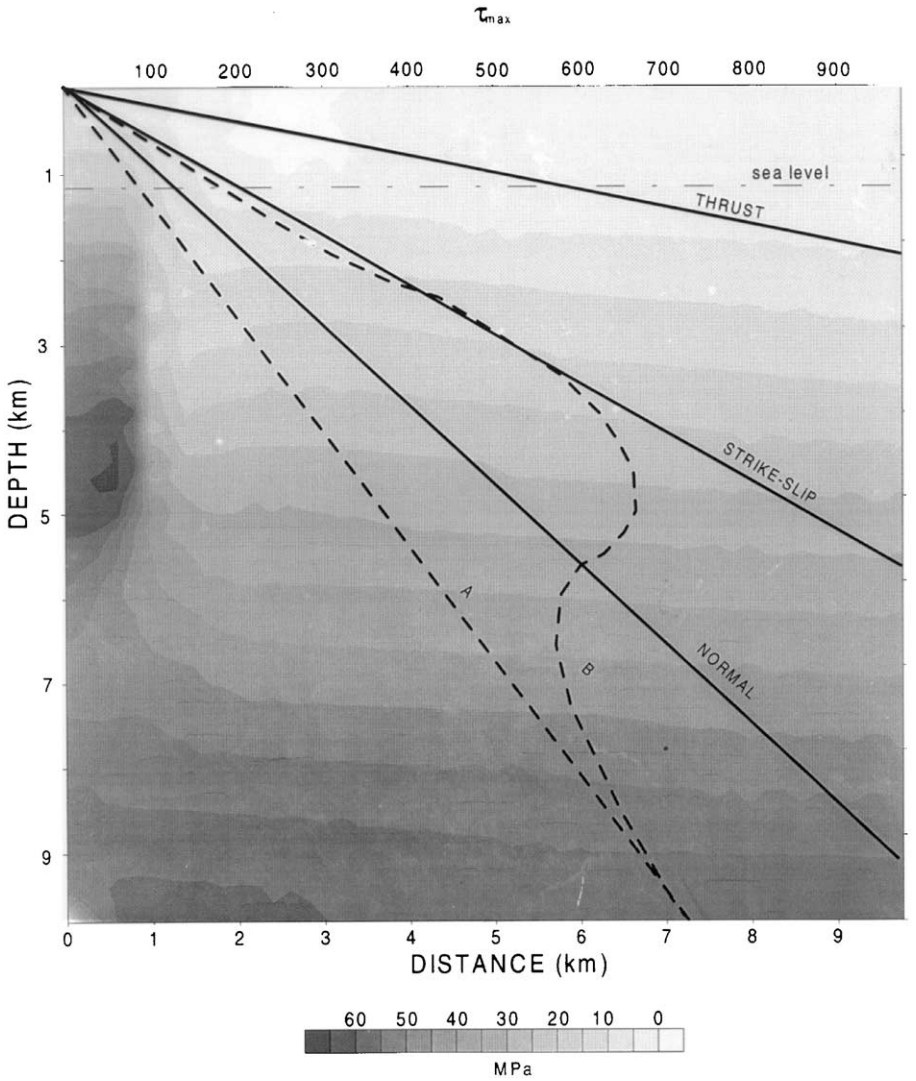

Fig. 12. Map showing the distribution of τ_{max} as computed for case I. Superimposed (continuous lines) are the expected curves for critical maximum shear stress before rupture, for the case of normal, strike slip and thrust mechanisms, as computed from laboratory experiments and theoretical considerations (from Hill, 1992 and references therein). Broken lines indicate the maximum shear stress computed in the case of a flat gravitating medium (A) and for the case I of Fig. 11 (B). Maximum stress means the maximum value computed at each depth, over all the distances from the central point. Curves of observed depth distributions of number of earthquakes and released seismic moment are also shown in the figure (bold lines), and show a very good correlation with the theoretical depths of maximum shear stress (after De Natale et al., 2000).

4.3. Evidence for opening of magma chamber, magma rising processes and timing, from rock texture analysis

The processes controlling the chemical–physical conditions for the opening of the magma chambers are poorly known, however integrated studies of eruptions and rock texture provide evidences on timing of the processes and chemical–physical conditions immediately before and during the eruption. Studies of deposits and/or direct observations of Somma–Vesuvius eruptions have furnished parameters such as total eruptive volume, mass eruption rate, duration of single phases, conduit size, etc (De Vivo et al., 1993). Recent rock texture studies (Mastrolorenzo et al., 2001) including abundance, shape, size distribution of vesicles provide constraints on the magma chamber/conduit processes in Campanian alkaline magmas.

Generally, Plinian and sub-Plinian eruptions which range in size between one to few cubic kilometers DRE and lasted for some tens of hours are characterized by mass effusion rate of 10^6–10^8 kg/s (De Vivo et al., 1993) by a conduit with dimension that ranges between a few tens of meters and about one hundred of meters (Sigurdsson et al., 1985; Lirer et al., 1993; Rosi et al., 1993;

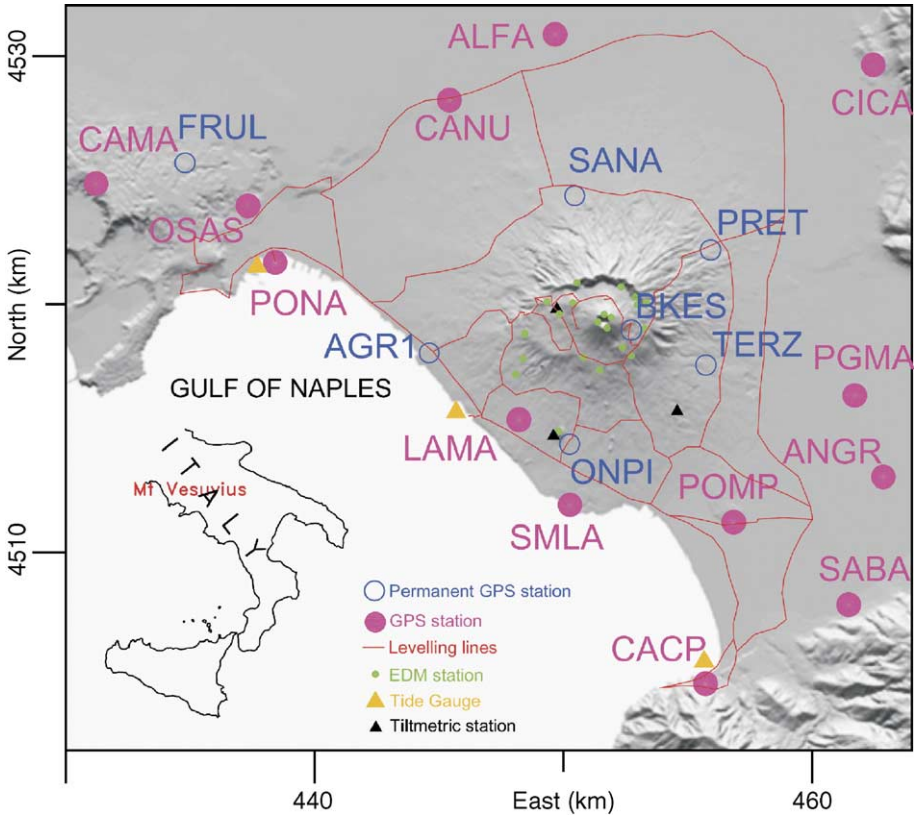

Fig. 13. Sketch map of the geodetic monitoring network at Somma–Vesuvius area.

Rolandi et al., 1993). On the contrary, open-conduit eruptions that range in size between a few millions and some hundreds of cubic kilometers DRE are characterized by mass effusion rate of 10^4–10^6 kg/s with a conduit with dimension in the order of few tens of meters (Mastrolorenzo et al., 1993; Scandone et al., 1986; Arrighi et al., 2001). These calculations include also the effusive phase in the order of few tens of cubic kilometers per second. In particular calculations carried out for the 1906 paroxysmal eruption of Vesuvius indicate that the average mass flux approached 1.7 millions kg/s with a maximum conduit radius of about 10 m (Mastrolorenzo et al., 1993). Modelling of the 1944 paroxysmal eruption indicates a maximum mass eruption rate of about 3.5×10^5 with a maximum conduit radius of about 4 m (Scandone et al., 1986). These results suggest that total volume of accumulated magma in the conduit is some order of magnitude less than that of the total erupted magma, that therefore must be stored at depth in the chamber. This implies that during an eruption, most of the magma have to pass trough the whole conduit length, mostly controlled by pressure gradients.

A comparative analysis of the vesicularity features of different types of most of explosive eruptions of Campanian alkaline rocks (Mastrolorenzo et al., 2001) reveals that in spite of different eruption size and eruptive style, bubble number density and bubble size distributions have similar values, thus suggesting that magma rising was always accompanied by intense vesiculation in conditions of diffusivity controlled regime in response to the pressure gradient. Magma degassing during movement to shallower depth is accompanied by microlite crystallization. Such crystallization requires no cooling, as decompression and attendant water loss shift the solidus to higher temperature. The rate of microlite crystallization could be defined by experimental and textural (Marsh, 1988) studies and used to constrain the timing of rising processes (e.g., Gardner et al., 1998; Hammer et al., 1999). According to Marsh (1988) and Cashman and Marsh (1988) the distribution of crystal sizes in rocks can be related to growth rate and residence time. They established that for a collection of crystals that have had a simple growth history, the natural logarithm of the crystal population density is inversely proportional to the crystal length. This line is

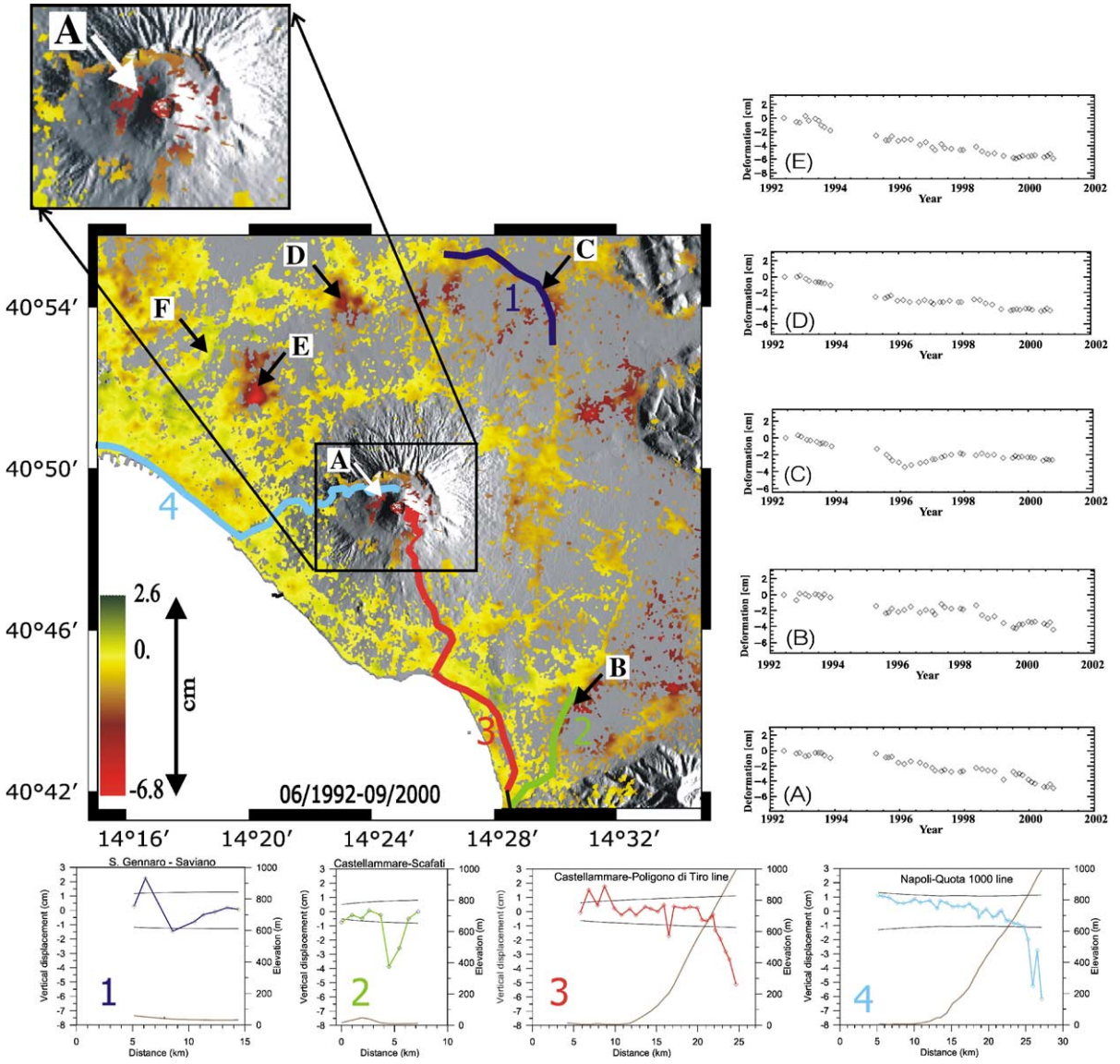

Fig. 14. Sketch map of the SAR, geodetic and seismic observations at Somma–Vesuvius. The base of the figure shows the DIFSAR false color deformation map, relative to the interval 06/1992–09/2000, computed in coherent areas only (in colours); the plots in the right column show the temporal evolution of the deformation for a few selected zones: (A) volcano summit, (B) Scafati area, (C) Saviano area, (D) Pomigliano d'Arco area, (E) Volla area. The light-blue and red lines, which end at the foot of the Vesuvius crater, as well as the green and magenta peripheral lines, are evidenced; displacements data on these four lines are reported in the separate boxes at the bottom of the figure, where topography (brown lines) and 95% level confidence (black lines) are also indicated. The Vesuvius cone is highlighted in the exploded box (upper left). (Redrawn after Lanari et al., 2002).

generally called the crystal size distribution (CSD). The slope of this correlation line is equal to $-1/GT$ (where G is the growth rate and T is the residence time) and the intercept is equal to the crystal nucleation density. Moreover rapid rates of undercooling result in high rates of nucleation and a dense population of crystals (CND).

Large Somma–Vesuvius Plinian events are characterized by microlite free to low content of microlites and by single slope in CSD. Moderate to high scale events ($0.01 \div 0.1$ km^3 DRE) show low CND and two slopes in CSD. Calculations based on these features indicate relatively fast magma rising in conditions of moderate-to-higher undercooling and degassing. As an example, in the climatic phases of the Vesuvius Plinian events, the magma rises in less than tens of minutes, a time comparable with the one calculated for the 1991 Mt Pinatubo eruption (Hammer et al., 1999). In all the calculations, estimated rising times range from minutes to hours. Fig. 16 shows the textural images and CSD of the products of 79 AD Vesuvius and 1991 Mt Pinatubo eruptions.

5. Probabilistic evaluation of volcanic hazard

The key issue for a highly explosive volcano like the Vesuvius, located in an extremely populated area, is the accurate estimation of hazard from eruptions, and its impact on the urbanised areas. Besides the large body of volcanological and geophysical research on Vesuvius, no global, accurate estimation of volcanic hazard in this area has been till now afforded in scientific literature. The lacking of a general method, well grounded statistically and volcanologically, to infer the hazard from eruptive products, has represented the main problem also for Vesuvius. Classically, preliminary inferences of hazard are based on the direct mapping of past eruptive products (Connor et al., 2001). Obviously, such a method is largely unsatisfactory because the past eruptive history, provided it can be well reconstructed, gives a very uneven and lacking sampling of the whole spectrum of possible eruptions, making meaningless any statistical assessment of hazard built on such a basis. Recently, Rossano et al. (2004) presented a rigorous volcanological–statistical procedure to build maps of hazard from pyroclastic currents. Their basic methodology can be easily generalised to build hazard maps for any kind of eruptive products. In the following, using a generalisation of the Rossano et al. (2004) approach, we will build the first probabilistic hazard maps for the Vesuvius from the two main kinds of eruptive products: pyroclastic currents and falls.

5.1. Pyroclastic density currents

The pyroclastic density currents (PDCs) simulation is carried out by direct and inverse numerical simulation of pyroclastic flows, based on a simple model of a gravity driven pyroclastic current which stops for en masse freezing (Rossano et al., 1996, 1998, 2004). The flow is assumed to be incompressible with a Newtonian or Bingham rheology. Emission from the vent is considered as steady state from the initiation of eruption.

The physical model of PDCs is described by the equations of uniform flow for a Bingham or Newtonian fluid (McEwen and Malin, 1989; Rossano et al., 1996). The steady, uniform velocity profile for a Bingham flow in infinitely wide channels is given by:

$$v(z) = \frac{1}{\eta}\left[\frac{\rho g \sin\theta (D^2 - z^2)}{2} - k(D - z)\right] \tag{1}$$

where $z \geq D_c$ is the height (measured from the bottom of the channel), k is yield strength, ρ is the density of flow material, g is acceleration due to of gravity, θ is the slope of ground, η is the viscosity, D the total flow depth, and D_c is the plug thickness,

$$D_C = \frac{2(kD + \eta v) - \sqrt{(2kD + 2\eta v)^2 - 4k^2 D^2}}{2k}. \tag{2}$$

The acceleration of the plug in a wide channel is (McEwen and Malin, 1989):

$$\frac{dv_p}{dt} = |a| - \frac{2k}{\rho(D + D_c)} - \frac{2\eta v_p}{\rho\left(D^2 + D_C^2\right)} \tag{3}$$

where v_p is plug velocity and $|a|$ is the modulus of the gravity contribution to the flow motion.

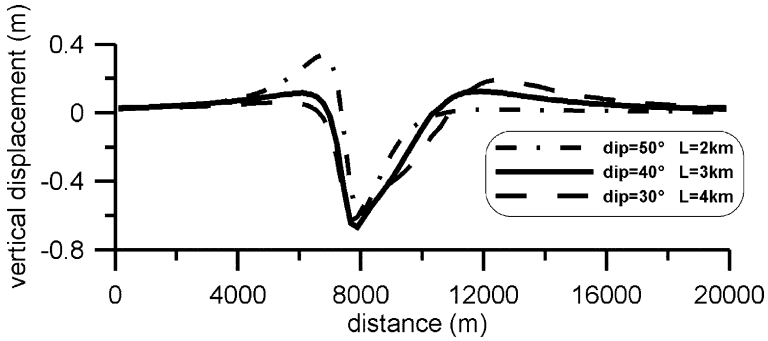

Fig. 15. Vertical displacements produced by normal faults of indicated dip and width (L), with top located at 1 km of depth and 1 m of fault slip (after Lanari et al., 2002).

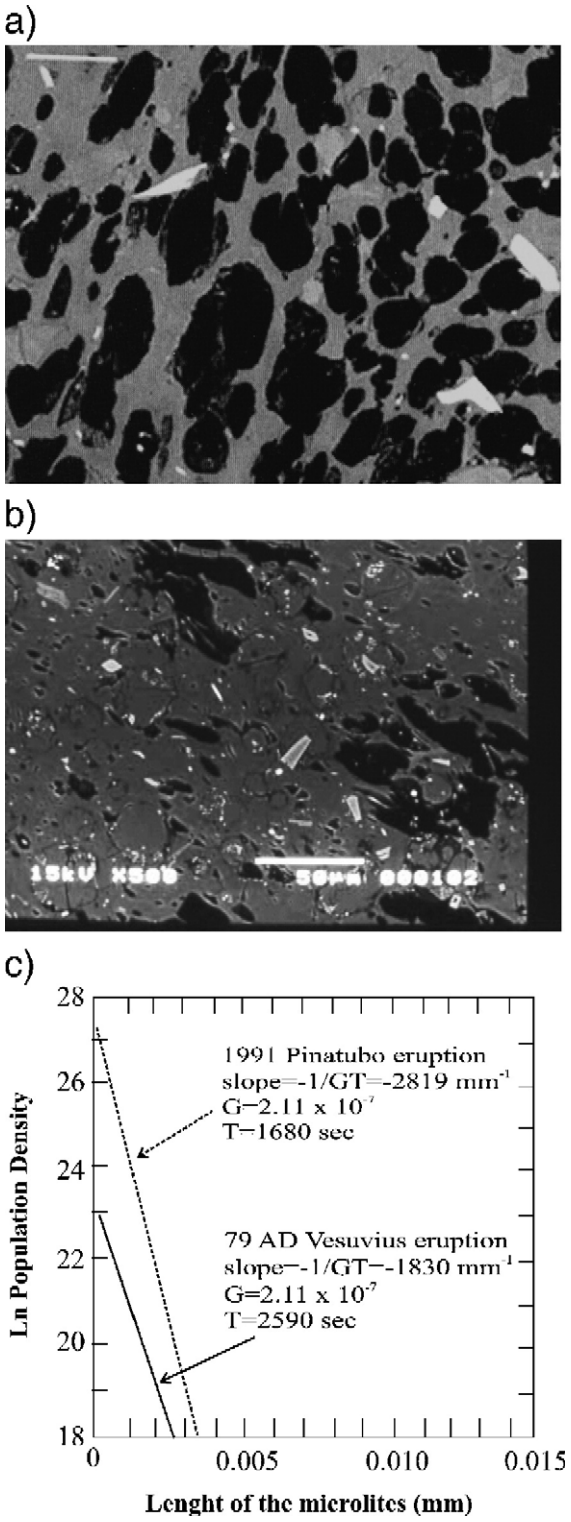

Fig. 16. Vesicle texture and microlites in explosive products of (a) Pinatubo Plinian eruptions; scale bar 10 μm and (b) 79 A.D. Vesuvius Plinian eruption; scale bar 50 μm. (c) Slopes of the relative CSD distributions ($-1/GT$), where G is the value of the crystal growth rate, T is the residence time as computed from the slopes. Both examples are relative to the climactic stages of the Plinian eruptions, however the products of the previous stages exhibit comparable CSDs. (After Mastrolorenzo et al., 2001).

Resistance terms in the equation describing a Bingham flow unit depends on several factors. For a Bingham flow, the transition from laminar to turbulent flow depends upon two dimensionless numbers, the Reynolds number $Re=\rho vD/\eta$, and the Bingham number $Bi=kD/\eta v$. From empirical relations, Middleton and Southard (1978) observed that, when Bi exceeds about 1.0 the onset of turbulence occurs for $Re/Bi \geq 1000$. According to McEwen and Malin (1989), we the frontal air drag is assumed to be negligible, so that the deceleration due to air drag on the upper surface (Perla, 1980) of the flow is:

$$\frac{dv}{dt} = -c_a\left(\frac{\rho_a}{\rho}\right)\frac{v^2}{2D} \tag{4}$$

with c_a ranging between 0.1 and 1 (Perla, 1980), The matrix of the input parameters for the generation of PDCs model set includes: vent coordinates, initial velocity and direction of the flow, flow density, thickness and rheological parameters (viscosity and yield strength).

In our simulation we compute the trajectories over a digital topographic model of Somma–Vesuvius of an idealised, one dimensional, mass-independent flow, approximated as a material point, representing the flow plug. The kinematics of the material point is governed by the equations reported above, with the known values of the local component of acceleration, and the assumed physical properties of the moving flow (initial velocity, density and rheology) and air friction. A large family of flow lines simulates the travel paths of a linear front departing from vent.

As discussed in previous papers (Rossano et al., 1998) even if we neglect lateral expansion, interaction between distinctive streamlines, effects of entrainment and sedimentation, the high density of 1D flow lines approximates a 2D model. This is particularly true for the high ratio between average PDCs thickness and small scale average landforms of the area.

We simulate a large number of individual 2D Pyroclastic Density Currents (PDCs) spanning a wide range of properties and vent conditions. Each 2D flow, characterised by specific physical properties, is defined by a family of 1D flow lines that move over a digital elevation model of Somma–Vesuvius and surroundings as a gravity driven current. The whole set of flow models is obtained by sampling a multidimensional matrix of vent position, initial velocity and rheological parameters which control the pyroclastic flow movement. Eqs. (1)–(4) have been used to simulate the flows.

In order to build meaningful hazard maps with the described procedure, accurate volcanological consideration of the past eruptions must be used to infer the matrix of variability of the parameters which define the pyroclastic currents. The values of the flow parameters must be then weighted, in the simulations, by their relative probability of occurrence, which can be in turn inferred by the relative frequency of the various kinds of eruptions, provided each eruption kind can be characterised by a given set of flow parameters. This choice of input parameters with relative weights represents the key factor in order to correctly extract all the volcanological information contained in the eruptive history of the area, and corresponds to assume that the relative frequency of the various eruption kinds observed in the past will be preserved in the future activity. In practice, the probabilistic method is used to build a much richer eruptive catalogue, which preserves the same statistical properties of the observed one.

As clear from the formulas, the parameters which characterise the single pyroclastic currents are the following: initial velocity, viscosity, density, thickness, yield strength. A huge work has been afforded in order to extract, from the observed eruptive catalogue, the ranges of parameter values characterising each eruption kind. The resulting scheme is synthesized in Table 1, which gives the matrix of central values of flow parameters, together with the

Table 1
Matrix of input parameters and their relative probability for Pyroclastic Density Currents (PDC) simulations at Somma Vesuvius

Parameters	Matrix of sampled input values (*and assumed relative probability*)						
Initial velocity (m/s)	2 (*2*)	5 (*3*)	10 (*5*)	20 (*10*)	50 (*20*)	100 (*40*)	200 (*20*)
Viscosity (Pa x s)	1 (*10*)	10 (*20*)	100 (*40*)	1000 (*20*)	10000 (*10*)		
Density (Kg/m^3)	5 (*5*)	10 (*10*)	100 (*50*)	1000 (*30*)	2000 (*5*)		
Yield strength (Pa)	0 (*40*)	100 (*25*)	1000 (*25*)	10000 (*10*)			
Flow thickness (m)	3 (*10*)	10 (*40*)	30 (*40*)	100 (*10*)			

occurrence probability, used in the framework of the probabilistic approach to build hazard maps. All the combinations of the given parameter values are considered in the simulation, each one taken with the cumulative probability given by the product of probabilities of the single parameters. The eruptive center is posed in the main crater, because lateral eruptions at Vesuvius are very rare (Santacroce, 1987). With these choices, hazard maps are computed by extracting, from the whole set of 2800 simulated eruptions, the probabilities of flow crossing of each given area of 1 km^2 on the topographic map. The crossing probabilities are computed as the sum of probabilities from each given eruption for which one flow at least crosses the area. The resulting probabilistic hazard map obtained is shown in Fig. 17.

5.2. Pyroclastic fall-out

The transport of tephra in the atmosphere, due to the processes of convection, diffusion and settling, may be described by the following well-known convection–diffusion–migration equation (Friedlander, 2000), written here in conservation form:

$$\frac{\partial \chi}{\partial t}+\frac{\partial u\chi}{\partial x}+\frac{\partial v\chi}{\partial y}+\frac{\partial w\chi}{\partial z}=\frac{\partial}{\partial x}\left(K_x\frac{\partial \chi}{\partial x}\right)+\frac{\partial}{\partial y}\left(K_y\frac{\partial \chi}{\partial y}\right)+\frac{\partial}{\partial z}\left(K_z\frac{\partial \chi}{\partial z}\right)-\frac{\partial V_{\mathrm{ts}}\chi}{\partial x} \tag{5}$$

where χ is the concentration of tephra ($\mathrm{kg}\cdot\mathrm{m}^{-3}$), $\mathbf{v}\equiv(u,v,w)$ is the wind velocity vector, K_x, K_y, K_z are diffusion coefficients, V_{ts} is the terminal settling velocity. In the hypothesis of low volume concentration of tephra, $\mathbf{v}$, K_i and V_{ts} depend only on (x, y, z, t) but not on χ so the equation is linear. Given an expression

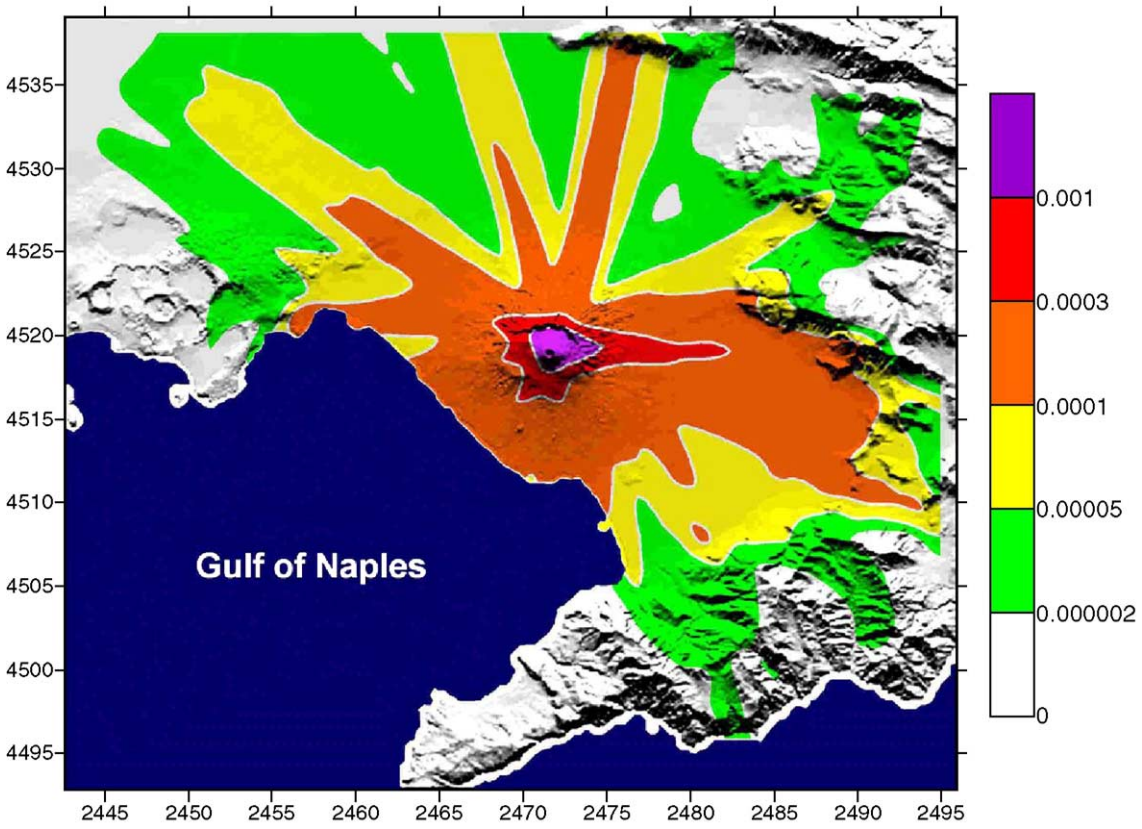

Fig. 17. Hazard map from pyroclastic currents at Vesuvius area, computed taking into account statistical distribution of eruption kinds during the past history. The value gives the probability for each area of a square kilometer, with center at the given point, to be hit by a pyroclastic current in a one-year interval.

for such coefficients and suitable boundary and initial conditions, Eq. (5) may be numerically solved to give $\chi=\chi(x,y,z,t)$. The mass distribution of tephra after all particles settled may then be calculated by the integration of vertical fluxes at the surface, at a time sufficiently higher than the settling time of the smallest particles we are interested in. However, such an approach is computationally expensive: in order to calculate the 2D distribution of tephra on the ground for $t_F>t_s$, we have to compute a 3D field for all times $t<t_F$. According to Suzuki (1983), we neglect vertical diffusion and convection in the atmosphere with respect to horizontal diffusion and convection because the former has a much smaller effect than the latter above the atmospheric boundary layer. We have:

$$\frac{\partial\chi}{\partial t}+\frac{\partial u\chi}{\partial x}+\frac{\partial v\chi}{\partial y}=\frac{\partial}{\partial x}\left(K_x\frac{\partial\chi}{\partial x}\right)+\frac{\partial}{\partial y}\left(K_y\frac{\partial\chi}{\partial y}\right). \tag{6}$$

Now χ has the meaning of mass of accumulated tephra for unit surface ($\mathrm{kg\cdot m^{-2}}$). The settling term is implicitly taken into account by considering the solution of Eq. (6) at the time corresponding to the fall time of particles. Diffusion is assumed to be isotropic ($K_x=K_y=K$), with wind velocity depending only on z, and diffusion coefficient constant in space and time. We write $K=C\cdot t^{3/2}$ with $C=0.04\ \mathrm{m^2 s^{-5/2}}$. K is not a turbulent diffusion coefficient but a partly empirical parameter, which takes into account all effects which tend to spread the plume, such as eddy diffusion, gravity flow, and so on. We assume the following boundary and initial conditions for Eq. (6):

$$\begin{aligned}&\chi(x,y,0)=Q\delta(x-x_0,y-y_0)\\&\lim_{r\to\infty}\chi(r,t)=0\qquad r=\sqrt{x^2+y^2}\end{aligned} \tag{7}$$

corresponding to the instantaneous release at $t=0$ of a mass Q from a vent of coordinates (x_0, y_0), in a doubly infinite domain, with the physical conditions that the concentration of tephra decreases at sufficiently high distances from the source. Then Eq. (6) has the following analytical solution:

$$\chi=\frac{5Q}{8\pi Ct^{\frac{5}{2}}}\exp-\left(\frac{5\left((x-ut-x_0)^2+(y-vt-y_0)^2\right)}{8Ct^{\frac{5}{2}}}\right). \tag{8}$$

In order to obtain the distribution of tephra to the ground, we set t equal to the fall time of the particle. To take into account the wind with z, let us divide the height of the atmosphere into layers of height Δz_i, characterized by constant wind velocity and direction. Particles in the eruption column have different diameters, and arrive to different heights into the column. Let us consider particles of grain size ϕ_j arriving at height z_k in the column ($z_k\le H$, total column height): they fall through layers $\Delta z_k=z_k-z_{k-1},\ldots\ \Delta z_1=z_1-z_0$, ($z_0=0$). Each layer is crossed in a time $\Delta t_i=\Delta z_i/V_{ts}(z_i,\phi_j)$, where terminal settling velocity V_{ts} depends both on height and on grain size, but not on time since we can assume that atmospheric density and viscosity at heights of kilometers are independent of time upon the time scales of tephra deposition. In this time, the center of the Gaussian distribution is displaced by $\Delta x_i=u(z_i)\Delta t_i$ and $\Delta y_i=v(z_i)\Delta t_i$. So, when the particles reach the ground, the distribution is:

$$\chi=\frac{5Q}{8\pi C\left(\sum_{i=1}^{K}\Delta t_i\right)^{\frac{5}{2}}}\exp\left(-\frac{5\left(\left(x-x_0-\sum_{i=1}^{K}\Delta x_i\right)^2+\left(y-y_0-\sum_{i=1}^{K}\Delta y_i\right)^2\right)}{8C\left(\sum_{i=1}^{K}\Delta t_i\right)^{\frac{5}{2}}}\right). \tag{9}$$

The tephra mass is distributed along the height of the column, and has a continuous grain size distribution. Summing on all heights from 0 to H (column height) and from minimum to maximum diameter, we get the complete grain size distribution:

$$\chi = \int_0^H \int_{\phi\min}^{\phi_{\max}} f_z(z,\phi) f_\phi(\phi) \frac{5Q}{8\pi C\left(\int_0^z \frac{dz}{V_{\mathrm{ts}}(z,\phi)} + t_s\right)^{\frac{5}{2}}} \exp\left(-\frac{5\left(\left(x - x_0 - \int_0^z \frac{u(z)dz}{V_{\mathrm{ts}}(z,\phi)}\right)^2 + \left(y - y_0 - \int_0^z \frac{v(z)dz}{V_{\mathrm{ts}}(z,\phi)}\right)^2\right)}{8C\left(\sum_{i=1}^K \Delta t_i\right)^{\frac{5}{2}}}\right) d\phi dz \tag{10}$$

f_z and f_ϕ are the distribution functions with respect to height and to diameter, respectively. To the diffusion time, we added the value t_s corresponding to the diffusion of particles inside the eruption column, due to the fact that the eruption column is not really a vertical line, but has a non-zero cross-section.

We use the semiempirical expression from Suzuki (1983) for t_s:

$$t_s = \left(\frac{5z^2}{288C}\right)^{\frac{2}{3}}.$$

We considered release from an instantaneous point source at time $t=0$ and position (x_0, y_0), while in reality an eruption has a defined duration and spatial extension. In order to understand its implications, we write a continuous eruption as the integral with respect to time of instantaneous emissions of intensity $I=\mathrm{d}Q/\mathrm{d}t$. This is possible in virtue of Duhamel's principle for parabolic linear PDEs, like Eqs. (5) and (6). If f_z and f_ϕ are independent of time, thus also total column height, maximum and minimum grain size, all quantities in Eq. (10) are independent of time, with the only possible exception of I. So we take everything except I out of the time integral, and, since the integral of I from 0 to t is equal to Q, we have precisely the same result that in the case of an instantaneous eruption. Physically, the reason is that we already assumed that transport phenomena in the atmosphere are independent of initial and final time, depending only on the difference between them, and also independent of particle concentration. So identical particles released at different time from the same height will stay in the atmosphere for the same time, and fall to the same place.

Thus we proved that in order to model a continuous eruption as in instantaneous release, we must assume that f_z and f_ϕ do not depend on time, i.e. to consider a quasi-steady eruption column. This assumption is valid for Plinian eruptions after the initial explosion (Woods, 1988).

In order to complete the mathematical description of our model, we must then specify:

(1) the way to compute terminal settling velocity;
(2) the functional form for grain-size distribution and for vertical mass distribution in the column.

In additional we must specify that probability distributions of wind velocities and directions have been taken from the measurements of the Brindisi (Southern Italy) meteorological station, in the period 1969–2000.

We supposed particles to fall always with its terminal settling velocity, i.e. we neglected transients, which is correct due to extension of the vertical layers in which we divide the atmosphere. The expression for the terminal settling velocity of a particle is a difficult point; when the velocity of the particle is equal to V_{ts}, drag force due to air and weight of the particle must balance:

$$m_p g = \frac{1}{2}\rho_a A C_d V_{ts}^2 \tag{11}$$

where m_p is particle mass, g is gravitational acceleration, ρ_a is air density, A is particle cross-section and C_D is a nondimensional parameter called drag coefficient, defined as the ratio between the aerodynamic drag force on the particle and the product of dynamic pressure $\frac{1}{2}\rho_a V$ for the cross-section A. C_D depends on the Reynolds number Re, defined as:

$$Re = \frac{\rho_a V d}{\mu} \tag{12}$$

where V is particle velocity relative to the air, d is particle diameter (mean of the three principal axes for aspherical particles), μ is air viscosity. If $Re \ll 1$, we are in Stokes regime, where, for spherical particles, $C_D = 24/Re$, so we get the following analytical expression for V_{ts}:

$$V_{ts} = \frac{\rho_p d^2 g}{18\mu}. \tag{13}$$

Outside Stokes regime ($Re \ll 1$), no analytical solution for V_{ts} has been found up to now, even for simple shapes like spheres. This is due to the nonlinearity of the Navier–Stokes equations, partial differential equations governing the viscous flow of Newtonian fluids like air. Experimental expressions are thus needed, but different set of experimental results for volcanic particles are often in disagreement. Suzuki (1983) found an expression which fits well different experimental data:

$$V_{ts} = \frac{\rho_p g d^2}{9\mu F^{-0.32} + \sqrt{81\mu^2 F^{-0.64} + 1.5\rho_a \rho_p g d^3 \sqrt{1.07 - F}}}$$

$$d = \frac{a+b+c}{3} \tag{14}$$

$$F = \frac{b+c}{2a}$$

where ρ_p is particle density, ρ_a is air density, a, b, c are the three principal axes with a being the longest, μ is air viscosity, F is called shape factor and is equal to 1 for spherical particles, d is the mean diameter.

Such an expression works well for low to moderate Reynolds number; in fact for $Re \to 0$ and $F = 1$ it becomes the Eq. (13), correctly. However, it fails for higher values, because it predicts a decreasing C_D, while experimental evidence for volcanic particles shows that the drag coefficient approaches the value 1 for high Re. We thus chose to compute the Reynolds number Re_L which, according to Suzuki's expression, corresponds to a drag coefficient of 1, and use Suzuki's expression for $Re \le Re_L$, while if $Re > Re_L$ we set $C_D = 1$ and obtain V_{ts} from Eq. (11). We write V_{ts} for a spherical particle, in order to show that V_{ts} increases with the diameter and the density of the particles:

$$V_{ts} = \sqrt{\frac{4\rho_p d g}{3\rho_a}}. \tag{15}$$

Air density and viscosity in the atmosphere depend on height, thus particles will fall quickly through the higher atmospheric layers, but will slow down at lower heights: the phenomenon is less important for the

smallest particles which move in the Stokes regime, their terminal settling velocity does not depend on density. We model the dependence of atmospheric thermodynamic properties according to the U.S. Standard Atmosphere 1976 (U.S. Government Printing Office, 1976).

We assume that the grain size distribution is lognormal, e.g. the distribution in ϕ units is normal ($\phi = -\log_2(d)$ where d is the particle diameter in millimeters):

$$f\phi(\phi) = \frac{1}{\sqrt{2\pi}\sigma_d}\exp\left(-\frac{(\phi-\mu_d)^2}{2\sigma_d^2}\right) \tag{16}$$

where μ_d and σ_d are respectively mean and standard deviation.

The vertical mass distribution in the column is taken from Connor et al. (2001):

$$f_z(z) = \begin{cases} \dfrac{\beta W_0 Y(z)\exp(-Y(z))}{V_{ts}(0,\phi)H(1-(1+Y(0)\exp(-Y(0))))} & 0 \le z \le H \\ 0 & \text{otherwise} \end{cases}$$

$$Y(z) = \frac{\beta W(z)}{V_{ts}(0,\phi)}$$

$$W(z) = W_0\left(1-\tfrac{z}{H}\right)^{\lambda} \tag{17}$$

where $W(z)$ is gas velocity at height z and W_0 is gas velocity at the vent. In this work it always assumed that $\lambda = 1$ since, according to Carey and Sparks (1986), linear variation of W with z is a satisfactory approximation for the major part of the column, except near the top and the bottom. From Eq. (17) it may be easily proved that the integral of f_z over $[0,H]$ is 1, and that $f_z \ge 0$ for any z, so it is indeed a distribution.

H is a normalization factor which does not change the shape of the function, so there are apparently three parameters b, W_0, $V_{ts}(0,f) = V_0$, in Eq. (17). However, f_z depends only on the product $Y(0) = \frac{bW(0)}{V_0} = b\frac{bW_0}{V_0} = Y_0$, so it is a one parameter distribution. In practice, W_0 and V_0 are constrained by the physics of the problem, so we study the dependence of f_z on β only. Omitting the simple but tedious calculation, we say that f_z has a maximum in $[0,H]$ if and only if $b^3 = \frac{V_0}{W_0}$. The terminal settling velocity at sea level of big particles is of the order of tens of meters for second, while the eruption velocity is of the order of hundreds of meters per second, so this condition is usually satisfied for all particles when $b^3 \approx 0.1$. The maximum is attained for $z_M = H\left(1\frac{V_0}{\beta W_0}\right)$ and has the value $f_z(z_M) = \frac{\beta W_0/V_0}{\varepsilon}\frac{1}{H\left(1-\left(1+\frac{\beta W_0}{V_0}\right)exp\left(-\frac{\beta W_0}{V_0}\right)\right.}$.

So we see that as $\beta \to \infty$, $z_M \to H$, $f_z(z_M) \to \infty$: since the integral of f_z must be 1, this means that larger values of β correspond to more mass being accumulated near the top of the column, and less at lower heights. We assumed $\beta = 0.1$, on the basis of several simulation t. The values of the other parameters assumed in these graphs are $H = 30$ km, $W_0 = 200\ \mathrm{m \cdot s^{-1}}$, spherical particles of density $\rho_p = 1000\ \mathrm{kg \cdot m^{-3}}$, standard air density and viscosity at sea level (see previous discussion on the terminal settling velocity).

Hazard maps are generated by simulating many eruptions, grouped in VEI (volcanic eruption index) 0 to 5, with distinctive probability according to volcanic history of Somma–Vesuvius.

The different values of eruption eruptions parameters for each VEI are assumed with distinctive probability according to the inferred features of past eruptions on the basis of the study of their deposits.

For each eruption of probability p, the height h of deposited tephra in each point (x_m, y_m) of the map is calculated from the grid (x_i, y_i) of the eruption, through change of coordinates and high order interpolation. For each (x_m, y_m), we assign h to one of m bins I_i covering all possible values, and add the probability p to the corresponding bin. Repeating this process for all eruptions, we obtain a probability histogram of the height of deposited tephra for each point (x_m, y_m). This gives the complete statistical description of the random variable h, so now we can compute the probability of h being higher than a given threshold, the mean value

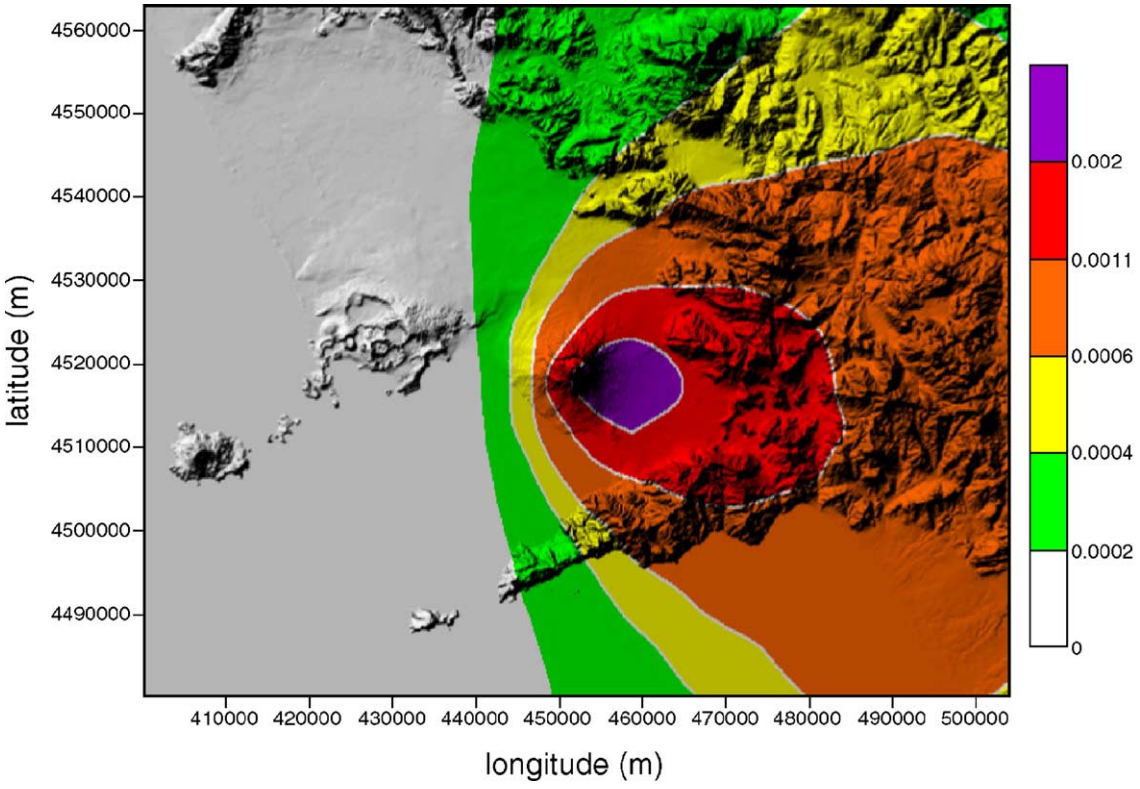

Fig. 18. Fall-out hazard map for Vesuvius eruptions. The maps are computed, by several tens thousands of computer simulations, on the basis of the observed wind velocity and direction between 0 and 35 km of height and their relative occurrence, considering all the eruption types with their statistics distributions, according to the volcanological records. The values are the yearly probabilities of a tephra load exceeding 200 kg/m^2 (producing the collapse of most roofs).

of h and so on, deriving the corresponding isomaps. The hazard map for tephra fall so computed is shown in Fig. 18.

6. Discussion

The recent research on Somma–Vesuvius has greatly increased our structural knowledge of the volcanic edifice and of the surrounding volcano–tectonic environment. At local scale, the structure of Somma–Vesuvius volcanic edifice shows some peculiar features, which are likely to be common to many central volcanoes. We can divide the velocity structure beneath the volcano in three main regions: a shallower one, consisting of the first 5 km of the crust; an intermediate one, from 5 to 15 km, and a deeper one down to the MOHO. Seismic tomography at local scale gives information about shallow depths; in particular, a high resolution picture of the first 5 km of the crust has been obtained. The most peculiar structure, evidenced in this depth range, is the presence of a high V_p (and V_s) anomaly along the volcano axis. This velocity anomaly indicates the presence of a high rigidity body, centred beneath the crater, with a lateral extension of less than 1 km. Such anomaly is spread towards W–SW at depths of 2–3 km. The high velocity of the central core of the volcano contrasts with the low velocity anomalies of the surrounding rocks, in particular those associated to the Somma caldera rims, in the Eastern sectors. While the low velocity anomalies of the external rocks are likely to represent compacted pyroclastic and fragmented products deposed on the slopes of the volcano, the character of the central, high rigidity anomaly should be associated to solidified and magnetized magma (Fedi et al., 1998) in the main volcanic conduits, accumulated during the whole life of the volcano. The extension of the high velocity anomaly, on the order of 5–7 km^3, suggests that it represents residual conduit solidified magma from one or more of the last cycles of activity of the volcano. However, the very short interval since the last eruptive cycle (1631–1944) and the very low values of thermal conductivity of the edifice rocks (Marsh, 1988), prevent

an interpretation in terms of substantial magma cooling. Convectional cooling models based on heat conduction through silicate rocks, with boundary layers at the margins of a chamber (Joupart and Tait, 1990), imply that residual molten magma should persist for much longer than few centuries after the end of activity.

A viable mechanism for accelerating solidification is magma quenching by volatile exolution. This mechanism has been recently proposed by De Natale et al. (2004a), and validated through laboratory analyses based on lava samples erupted in 1944. In the last years, such a structural signature, namely high rigidity along or near the crater axis, has been inferred at many other volcanoes world-wide (McNutt, 1996; Chiarabba et al., 2000). Its mechanical implications are very important, and probably characterise the dynamics of several central volcanoes worldwide. In fact, the presence of the strong rigidity contrasts along the crater axis acts to concentrate the local and regional stresses around such anomaly. The strong stress concentration in turns generates local seismicity highly clustered around the crater axis. The high clustering of seismicity around the central axis is very evident, at Vesuvius and also at several central volcanoes all over the world (McNutt, 1996; De Natale et al., 2000). De Natale et al. (2000) performed detailed modelling, recalled here, to show how the presence of the central rigidity contrast concentrates stress at the borders of the anomaly itself.

Below such high rigidity anomaly, namely below a depth of about 5 km, earthquake data give no information, because of the absence of seismicity and hence of seismic ray sampling. Neither active data give direct information, because transmitted waves generated at surface by shots are strongly channeled by the presence of the high velocity carbonatic platform (2–3 km of depth) so being not able to sample higher depths. The seismic information about the deeper structure comes from reflected waves of active sources and from P–S converted waves of teleseisms. Such data point to the evidence for a rather large conversion horizon, likely to represent a magma sill, at about 12–15 km of depth. No clear reflection–conversion layer of considerable dimension is imaged at smaller depths.

A marked decrease of V_s velocity in the depth-range 9–17 km is also imaged by Natale et al. (in press) from surface wave dispersion analyses. Although the inferred values of V_s would seem not consistent with the presence of considerable percentages of fluid magma, the large width of the low V_s interval, likely due to the investigated wave periods, could indicate that the effect of a sharper and narrower V_s minimum, compatible with magmatic velocities, has been spread over a broader interval.

Geochemical evidence of crystallisation depths, however, indicates the presence, at about 4–6 km of depth, of a typical zone of accumulation of magma, giving rise to the main Plinian and sub-Plinian eruptions of the past. Such shallower chamber doesn't necessarily contain magma at present, but some indirect evidences indicate that it anyway represents a zone of rigidity contrast. The main evidence is constituted by the depths of local earthquakes, which are strongly clustered at 4–5 km, which a marked peak of seismic moment release at this depth (Presti et al., 2004). As discussed by De Natale et al. (2000) such a clustering is in agreement with the presence, at this depth, of a zone of marked gradient of rigidity, coincident with the bottom termination of the central high rigidity anomaly. Other indications for the presence of a transition zone at this depth comes from geoelectric and magnetotelluric results (Di Maio et al., 1998). The main reflection–conversion horizon, evidenced by seismic waves, represents a magma body located at intermediate depth, which is also in agreement with one of the crystallization depths inferred by geochemical–isotopic data. Such data indicate, for eruptions of intermediate cycles, i.e. of energy smaller than Plinian or sub-Plinian ones, a depth range of crystallization of 10–22 km. The top part of this range agrees with the seismically inferred sill-like magma body, whereas the wide range partially overlaps with the deeper magma roots as inferred from regional teleseismic tomography. The complete picture which comes out from the recent studies is then the presence of three main depths of magma accumulation at least, one very shallow (4–6 km) feeding the Plinian and sub-Plinian eruptions, another one located at 10–15 km, forming a sill-like structure probably at the contact between carbonatic rocks and crystalline basement. Below 15 km of depth, teleseismic tomography put in evidence a velocity low in the range 15–30 km, possibly indicating the deeper magma roots feeding the upper crustal reservoirs on the basis of geochemical evidence of magma storage at 20 km. An interesting question regards the extension of the upper crustal reservoirs. A paper by Auger et al. (2001) claims that the intermediate depth magma sill would extend for an area of 400,000 km^2 at least, probably more. We believe that it is not easy to have a definitive proof for such a large area involved, nor can we constrain it with our data. Anyway, geochemical inferences point out similar crystallisation depths also for products of Campi Flegrei and Procida (De Astis et

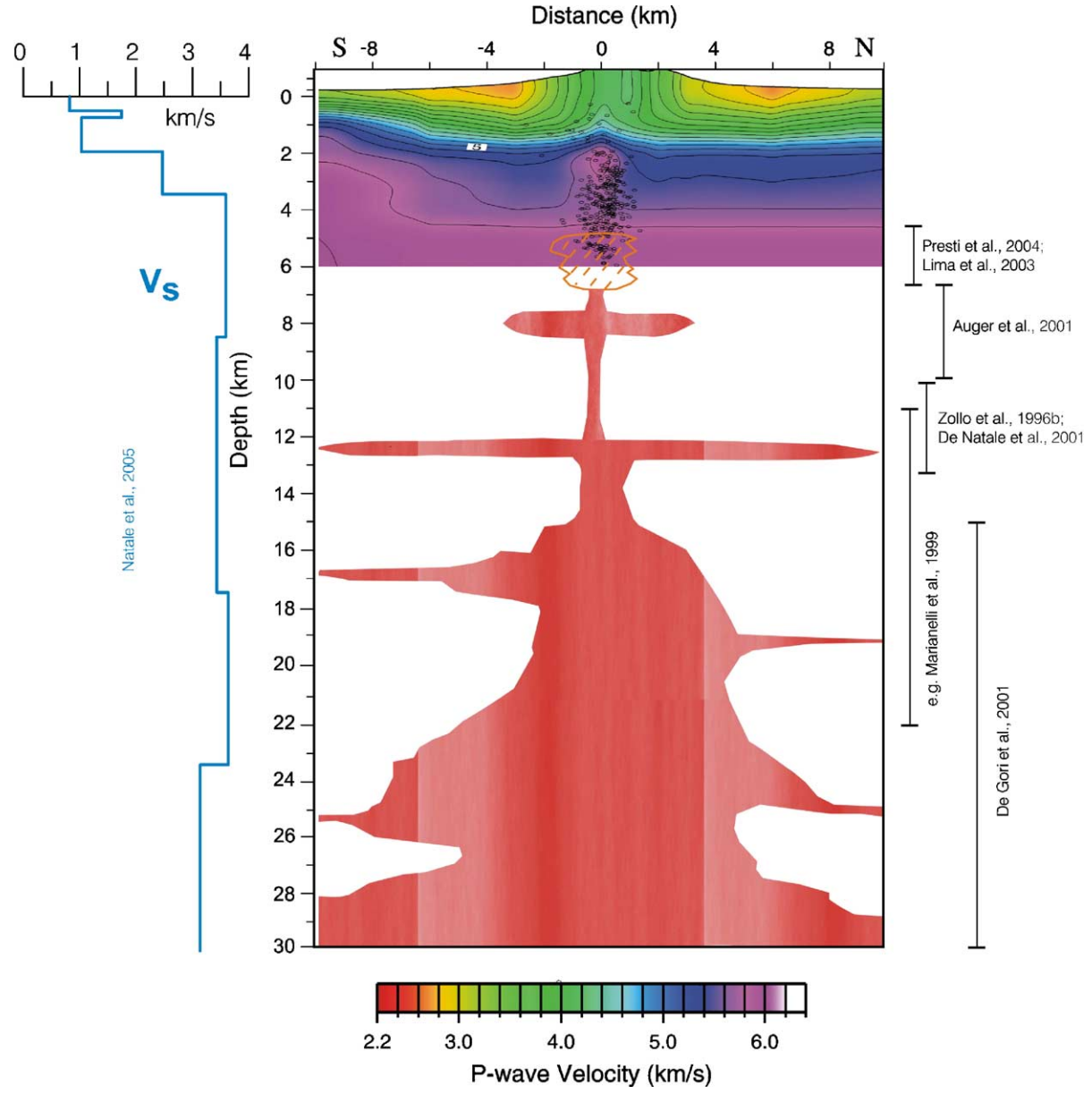

Fig. 19. Sketch map of the Somma–Vesuvius sub-structure, as reconstructed in this paper and also summarising the main inference on magma chamber depths and wave velocities as reported by recent geophysical and petrological literature. The shallow structure as determined by De Natale et al. (2004a) by joint tomographic inversion of shot and earthquake data is shown by a colour scale. Depth ranges inferred by different authors for the main magma accumulation zones are shown at the right, together with reference papers. The model for Vs velocity in the whole depth range, as recently determined by Natale et al. (2005) is also reported. The schematic picture of the hypothesized magmatic systems below 5 km of depth is only indicative.

al., 2004), thus suggesting this reservoir could be effectively widespread below the whole Campanian volcanic area. On the contrary, the shallow depth reservoir should be small, because it is not evident from seismic wave analyses. The shallower depth inferred, however, is very similar to that inferred, from seismic data, at Campi Flegrei caldera (Ferrucci et al., 1992; De Natale et al., 2001). Thus, it would imply that the formation of very shallow reservoirs in this depth range is a typical feature in this area, although they appear localised just below the individual volcanoes.

A complete sketch of the shallow Vesuvius structure and proposed magma chamber locations, as resulting from recent literature, is shown in Fig. 19.

Once the main depths of magma reservoirs are determined by the joint interpretation of seismic and petrological data, an important question for assessing future pre-eruptive scenarios concerns the determination of typical times for magma migration during eruptions, from upper crustal reservoirs to the surface. For Plinian and sub-Plinian eruptions, these times, determined from the density and size of microlites, which only form in the interval between the onset of migration and the eruption, turn out to be on the order of minutes to tens of minutes, slightly smaller than, for instance, the estimates for the 1991 explosive eruption from Pinatubo (Philippines).

Regarding the regional structure, the recent work of De Gori et al. (2001), in the framework of the BROADVES experiment, shed light on important structural and geodynamical questions. In particular, a very important finding for the understanding of geodynamic models and for the interpretation of the Thyrrenian volcanism, is the evidence in this area for a marked high velocity anomaly (up to 5% velocity perturbations) dipping under the Apennine chain. Such anomaly, much evident in the section of Fig. 7, is likely to represent a subducting slab, and represents the first evidence for a continuous subducting slab also at these latitudes. In previous works, Amato et al. (1993), had hypothesised a 'slab-window' in this area, implying the absence of subduction in the first 200 km of depth. Other works also indicate the Southern end of Campania as the northern limit of the subduction (Panza and Romanelli, 2001 and references therein). According to our recent work, on the contrary, this area seems to be characterised by the same continuous subducting slab which has been recently inferred along almost all the Apennine chain (Selvaggi and Amato, 1992; Cimini and De Gori, 1997) reconciling with petrological data indicating a slab-enriched mantle source (Peccerillo, 2001). The presence of subduction under the Campanian volcanoes could also be the key to understand the mechanism for the origin of the Thyrrenian and Campanian volcanism, an argument still opened to scientific debate. The seismic tomography at a regional scale, performed by the BROADVES, also put in evidence an important low velocity anomaly under Somma–Vesuvius volcano. Such feature is strongly constrained by the broad-band instruments installed in BROADVES experiments, and could not be seen before. The maximum velocity decrease below Somma–Vesuvius complex amounts to 3%, and extends in the layer located between 15 and 35 km of depth. The low velocity beneath the Vesuvius suggests the presence of a magmatic reservoir in the lower crust underneath the volcano. As already said, the low velocity zone can be interpreted as the deeper root of the upper crustal magmatic layer.

A more pronounced low velocity body (−5%) is imaged in the lower crust (layer 2) and in the uppermost mantle (layer 3) beneath the Roccamonfina volcano. We interpret this crustal feature as a possible deep magmatic chamber.

The lower crust beneath the western part of the Campanian Apennines is dominated by positive anomalies along the NW–SE direction that can be related to the basement of metamorphic rocks. This high velocity rim appears interrupted by the low velocity region observed from Roccamonfina volcano to the Bradanic foredeep (Fig. 6). The NE–SW trend of this low velocity corresponds approximately to the Ortona–Roccamonfina line, interpreted as a lithospheric free boundary separating the northern and the southern Apennines (Patacca and Scandone, 1989).

The low velocity zone reconstructed in the lower crust beneath the belt and the Bradanic foredeep (Fig. 6) matches the negative perturbations found by Chiarabba and Amato (1996) and Di Stefano et al. (1999) at 22 km depth. The location of this slow anomaly corresponds to a region of negative Bouguer anomalies, suggesting the presence of low density material or a thermal anomaly. An alternative interpretation could be the subduction of the continental Adriatic lithosphere beneath the Apenninic belt (Doglioni et al., 1994). This process may generate the observed crustal low velocity body by ascent of fluids coming from dehydration reactions in the subducted crustal materials.

Present dynamics of Somma–Vesuvius is mainly characterised by the occurrence of local earthquakes, having maximum magnitudes of 3.7. Such seismicity is persistent, with typical rates of some hundred events/year, with swarms also one order of magnitude larger, as occurred in 1989, 1995–1996, 1999–2000. Earthquakes are densely clustered around the high rigidity anomaly at the crater axis.

The presence of such a shallow structural anomaly, in conjunction with the gravitational load, mostly uncompensated, of the volcanic edifice, can explain this peculiar feature typical of many other central volcanoes, i.e., the background seismicity. Several central volcanoes, in fact, including Vesuvius, are characterised by a background level of seismic activity, which is present also during the quiescent periods of the volcano. The background seismic activity can be explained, in the framework of the De Natale et al. (2000) model, as due to the gravitational load of the volcano itself, which is able to bring the value of shear stress in the edifice very close or above the rupture threshold for host rocks. Small stress

perturbations, caused by internal sources or by regional stress changes, can thus generate background seismicity.

Further effects could be ascribed to pore pressure changes and/or sudden vaporization (explosion) of geothermal water in the shallow aquifers (Del Pezzo et al., 2004; De Natale et al., 2004b). Del Pezzo et al. (2004), based on the apparent depth-dependent variation of stress drop, hypothesize that seismic activity at shallowest levels is associated to local stress, whereas deeper earthquakes are mainly due to regional stress. Their model, however, is biased, in our opinion, by the fact that stress drop change is only apparent, and due to the mentioned constancy of apparent corner frequency in seismic spectra, likely due to strong site effects (Vilardo et al., 1996; Capuano et al., 1999). This effect, associated to a larger release of seismic moment at maximum depths (Presti et al., 2004) causes the apparent depth-dependence of stress drop. In our model, seismicity is mainly linked to local stress focusing, with the occasional superposition of local stress changes.

Seismic activity at Somma–Vesuvius can then be seen as consisting of a background level, mainly due to the instabilities caused by gravitational load and small external stress perturbations, with superimposed occasional episodes of stronger activity (De Natale et al., 2000). The occurrence of such strong seismic activity episodes is of major volcanological interest, because they are not simply associate with the background activity, but testify an increased dynamics which is most likely of internal origin. The energy release and b variation curves shown in Fig. 8 put in evidence, furthermore, a progressive increase of the energy rate and decrease of b value during the unrest episodes, starting from a very modest one occurred in 1977–1982 (about 10^{16} erg/year), to the maximum rate occurred at the end of 1999 (1.3×10^{17} erg/year) (De Natale et al., 2004b). A progressive decrease of the b value, on the other hands, is consistent with a progressive coalescence of fractures as observed in laboratory experiments during increasing loading of rock materials (Meredith et al., 1990). Seismic unrest episodes like those occurred in 1989, 1995–1996 and 1999 could be then a key to interpret the present state of internal dynamics of this volcano, and should be carefully considered and studied in the future research, mainly because of the extremely high risk in the area.

Static deformations at Somma–Vesuvius do not involve the whole edifice, which appears very stable, except for the crater area, in the last 30 yr at least. Localised ground subsidence is observed in the crater area, with rates in the range 0.5–1.0 cm/yr. Such a subsidence is consistent with the seismic behaviour of the area as inferred from our model, where gravitational instability produces earthquakes along the crater axis. Out of the volcanic edifice, a ring zone of subsidence is evident, surrounding the volcano, with yearly rates similar to those inferred for the crater area. The mechanism for such peculiar pattern of subsidence should be related to the joint effect of the tensional regional stress and the gravitational loading of the volcano, inducing ring normal fault-like slip along the low dip angle contact surfaces between volcanic and external rocks (Lanari et al., 2002). This kind of ring subsidence seems to be common to many other volcanoes, as first pointed out by Terada (1929) and also evident from topographic relief at Mt. St. Helens (U.S.A.). At these volcanoes, repeated subsidence of this kind has produced ring topographic depressions around the edifices, which is not the case for Somma–Vesuvius. The lack of topographic markers of the on-going deformation should be due, here, to the surface coverage of alluvional deposits, which cancel in the long term the traces of subsidence. Anyway, it is interesting to note that, recently, Lomax et al. (2001) found evidence from shallow seismic reflection studies of zones of depression of the carbonate basement, which are well correlated with the position of the subsiding ring. Such a peculiar depression of the basement is likely to represent the cumulative record of the long term subsidence, which is not present in the incoherent shallow soils but in the compact basement.

The pattern of static deformation at this volcano comes anyway mainly by about 30 yr of monitoring with progressively increasing levelling and EDM networks, and more than 10 yr of monitoring with GPS techniques. Recently, a paper by Borgia et al. (2005) hypothesised that the activity of Vesuvius is progressively decreasing, due to the on-going process of volcanic edifice spreading. Their hypothesis was mainly based on the spatial pattern of some ground deformation data, which was interpreted in terms of a spreading model.

On the contrary, the complete set of ground displacement data (both land-based and InSAR), clearly shows a pattern very different from what needed to advocate a spreading model, because the volcanic edifice is substantially stable except the central crater (Fig. 14). Furthermore, there is not trace of substantial uplift at the basis of the volcano, which would be produced by edifice spreading. On the contrary, the basis of the edifice is marked by the already discussed ring-like subsidence, which is at odds with respect to a spreading model. Besides the pattern of ground deformation, which do not support an interpretation in terms of

edifice spreading, the deduction of Borgia et al. (2005) which the volcano would be progressively decreasing its explosivity is strongly in contrast with the simple volcanological evidence which the eruptive activity in the last 3500 yr has been the most intensely explosive of the whole life of the volcano (Santacroce, 1987; Rossano et al., 1998).

The present knowledge about the structure and dynamics of the volcano, as synthesised in this work, allows to give some guidelines about the best strategies for monitoring the volcano, and about the most likely pre-eruptive scenarios.

On the other hands, the existence of a considerable level of background seismic activity, culminating in occasionally high energy unrests, will not help to recognise future patterns of pre-eruptive seismic activity. At Mt. Vesuvius, in fact, there is no historical or instrumental evidence for large earthquakes preceding eruptions. The maximum estimated magnitudes in the past are around 4, i.e., not really distinguishable from the most recent largest earthquakes (Ml=3.7), except for the 63 A.D. earthquake, occurring however long before (16 yr) the 79 A.D. eruption. The best choice for seismic monitoring aimed to forecast future eruptions should be then to optimise the possibility to discriminate earthquakes linked to fluid-magma movements from volcano-tectonic ones. Given the low frequency character of earthquakes and tremors due to magma movements (Chouet, 1996), broad-band sensors should be extensively deployed on this volcano. A further limitation to the use of monitoring magma migration comes from the very small duration of this process as inferred from microlite studies. Orders of magnitude of minutes to hours for magma rising before the eruption are not enough for detecting the first signals of rising to be of some utility for civil defence purposes. Anyway, the inference that Plinian and sub-Plinian eruptions should be fed by the shallowest magma chamber, located at 4–6 km of depth, suggests that a powerful method for assessing the hazard for major eruptions is detecting signals of shallow chamber filling, which can be deeper low frequency earthquakes, volcano-tectonic earthquakes surrounding the chamber or static deformations.

The low level of static deformation of the volcanic edifice observed till now, except for the crater area, prevents to make detailed considerations on the expected deformations accompanying future eruptive activity. We can say that the actual coverage of levelling lines and GPS networks, densely sampling the volcano and arriving at large distances and stable areas (Apennines), allows, in principle, a good monitoring and interpretation of any realistic pre-eruptive pattern caused by magma sources. Anyway, the minimum amount of deformation allowing to make meaningful interpretations should be on the order of some centimeters. Based on the high values of rigidity of the volcanic rocks inferred from seismic studies, mainly in the central part, some authors (Russo et al., 1997) hypothesize very low displacements (some millimeters) also for considerable intrusion sources. From our results, the area which should be more sensitive, in terms of ground deformations produced by intrusion sources, is the crater area, because the contact between the axial high rigidity rocks with the softer outer deposits is likely to be marked by fracture systems, as testified by the very localised crater subsidence and related seismicity. Magma inflow in the shallowest magma chamber should anyway generate detectable static deformation, given the low depth.

Previous considerations help to shed light on the possible pre-eruptive behaviour of the volcano. Anyway, besides the forecast of future eruptive activity, the most crucial information for risk mitigation is the precise evaluation of the major volcanic hazards. In this paper, we have shown the results of a new procedure for building probabilistic hazard maps for the two major sources of hazard from this volcano. The maps take into account the hazard from pyroclastic flows, which are by far the most destructive volcanic products, and the pyroclastic falls, which represent a considerable risk also very far from the eruptive vent, particularly for large Plinian eruptions.

Pyroclastic flow hazard maps show some interesting features, regarding the maximum hazard areas. In fact, they show that, besides the areas very close to the crater, the hazard maxima tend to be elongated East of the main crater, up to the Apennine chain, including the Sarno valley and the towns of Nola to North and Torre Annunziata to the South. The high hazard in this area is mainly due to the focusing of pyroclastic flows in the Sarno Valley, due to the confining effect of the valley and the Apennines. The same area is also deeply affected, for the same reasons, by secondary flows hazard, i.e. by post-eruption mobilisation of accumulated pyroclastic products, as practically demonstrated by the dramatic flooding due to landslides in the Sarno valley in 1999 (Mastrolorenzo et al., 2002). The other urbanised areas subject to highest hazard from pyroclastic flows include the coastal areas of the volcanic edifice, and, a large part of the city of Naples. In addition, some narrow channels pointing roughly North of the crater also show considerable hazard, due to flow channelling effects in Somma slopes gullies. The very interesting aspect of these maps is that, since they represent the first physically and statis-

tically based description of pyroclastic flow hazard, with a robust volcanological background, they can be of invaluable help in the building of average-long term urbanisation plans and of emergency plans, for civil defence purposes.

Pyroclastic fall hazard maps built with the analogue statistical procedure used for pyroclastic flow hazard maps show that the areas of highest hazard for tephra accumulation exceeding the limit for roof collapse (>200 kg/m^2) is spread in the eastern sectors because of dominant winds.

Its inferred occurrence is 3–5 time/kyr, 1 time/kyr, 0.6 time/kyr within 10 km, 40 and 100 km from the crater, respectively.

An important aspect of fall hazard maps is that, due to the dominance of western winds in the area, the city of Naples could be almost unaffected by the risk of roof collapse.

7. Conclusions

The recent geophysical research at Somma–Vesuvius, integrated with key geochemical evidences and new modelling results, allows to build a detailed picture of the main structural and dynamical features, as well as to constrain the hazard from eruptive scenarios.

The emerging picture is a volcano whose shallow structure is composed by a central high rigidity core made by still hot, degassed magma, whose lower termination ends with a ductile zone, marked by the abrupt termination of local earthquakes. This ductile zone is probably the upper part of a shallow magma chamber, which is likely to feed the most explosive eruptions. The recent dynamics is dominated by these shallow features: shear stress and consequent seismicity strongly cluster around the high rigidity body, and recent deformation involves subsidence of the upper expression (crater area) of this anomalous body. The reason for such apparently contradictory result (high rigidity should have low deformation associated) is the detachment of the younger Vesuvius crater from the ancient Somma structure, and possibly a lower effective rigidity of the axial boby for long term stress, involving viscoelastic rehology due to still high temperature. A large magma sill, located at about 10–12 km of depth and probably involving a large part of the Campania Plain, represents the main magma body feeding eruptions at this area. Deeper magma roots in this area are evidenced between 15 and 30 km of depth. The shallow structural features of this volcano are likely to affect also the pre-eruptive patterns, which are likely to consist in increased seismicity rates, low frequency earthquakes and static deformation which should be mainly pronounced within the rims of the ancient Somma caldera, for the same reasons which cause the present marked subsidence.

Finally, the use of new probabilistic procedures for hazard maps computation allow to define, for the first time on well grounded volcanological, physical and statistical bases, the hazard from pyroclastic flows and falls from Vesuvius eruptions. From these maps, new important information comes out on the most exposed areas, which could considerably change the actual point of view for emergency plans.

In conclusion, this paper gave the first large, multidisciplinary and consistent overview of the main constraints on Vesuvius activity, regarding structural elements, dynamics, possible pre-eruptive scenarios and probabilistic estimation of eruption hazard. Many results obtained at Vesuvius can be very useful to study and interpret the activity at other volcanoes world-wide.

Acknowledgements

We thank Giuliano Panza for constructive criticism and useful suggestions, which greatly improved the quality of the paper. We also thank an anonymous referee for useful criticism.

Paper partially supported by MIUR-FIRB 2001 funds (RBAU01M72W_001).

References

Amato, A., Alessandrini, B., Cimini, G.B., Frepoli, A., Selvaggi, G., 1993. Active and remnant subducted slabs beneath Italy: evidence from seismic tomography and seismicity. Ann. Geofis. XXXVI, 201–214.

Appleton, J.D., 1972. Petrogenesis of potassium-rich lavas from the Roccamonfina Volcano, Roman Region, Italy. J. Petrol. 13 (3), 425–456.

Arrighi, S., Principe, C., Rosi, M., 2001. Violent Strombolian and subPlinian eruptions at Vesuvius during post-1631 activity. Bull. Volcanol. 63, 126–150.

Auger, E., Gasparini, P., Virieux, J., Zollo, A., 2001. Seismic Evidence of an extended magmatic sill under Mt. Vesuvius. Science 294, 1510–1512.

Barberi, F., Leoni, L., 1980. Metamorphic carbonate ejecta from Vesuvius Plinian eruptions: evidence of the occurrence of shallow magma chambers. Bull. Volcanol. 43 (1), 108–120.

Belkin, H.E., De Vivo, B., 1993. Fluid inclusion studies of ejected nodules from Plinian eruptions of Mt. Somma–Vesuvius. J. Volcanol. Geotherm. Res. 58, 98–100.

Belkin, H.E., De Vivo, B., Roedder, E., Cortini, M., 1985. Fluid inclusion geobarometry from ejected Mt. Somma–Vesuvius nodules. Am. Mineral. 70, 288–303.

Berrino, G., Coppa, U., De Natale, G., Pingue, F., 1993. Recent geophysical investigation at Somma–Vesuvio volcanic complex. J. Volcanol. Geotherm. Res. 58, 239–262.

Berrino, G., Corrado, G., Riccardi, U., 1998. Sea gravity data in the gulf of Naples: a contribution to delineating the structural pattern of the Vesuvian area. J. Volcanol. Geotherm. Res. 82, 139–150.

Bertagnini, A., Landi, P., Rosi, M., Vigliargio, A., 1998. The Pomici di Base Plinian eruption of Somma–Vesuvius. J. Volcanol. Geotherm. Res. 83, 219–239.

Borgia, A., Tizzani, P., Solaro, G., Manzo, M., Casu, F., Luongo, G., Pepe, A., Berardino, P., Fornaro, G., Sansosti, E., Ricciardi, G.P., Fusi, N., Di Donna, G., Lanari, R., 2005. Volcanic spreading of Vesuvius, a new paradigm for interpreting its volcanic activity. Geophys. Res. Lett. 32 (3), L03303. doi:10.1029/2004GL022155.

Capuano, P., Coppa, U., De Natale, G., Di Sena, F., Godano, C., Troise, C., 1999. Accurate analysis of some local earthquakes at Somma–Vesuvius. Ann. Geofis. 42 (3), 391–405.

Carey, S.N., Sparks, R.S.J., 1986. Quantitative models of the fallout and dispersal of tephra from volcanic eruption columns. Bull. Volcanol. 48, 109–125.

Cashman, K.V., Marsh, B.D., 1988. Crystal size distribution (CSD) in rocks and the kinetics and dynamics of crystallization. Contrib. Mineral. Petrol. 99, 292–305.

Chiarabba, C., Amato, A., 1996. Crustal velocity structure of the Apennines (Italy) from P-wave travel time tomography. Ann. Geofis. 39, 1133–1148.

Chiarabba, C., Amato, A., Boschi, E., Barberi, F., 2000. Recent seismicity and tomographic modelling of the Mount Etna plumbing system. J. Geophys. Res. 105, 10923–10938.

Chouet, A.B., 1996. Long-period volcano seismicity: its source and use in eruption forecasting. Nature 380, 309–316.

Cimini, G.B., De Gori, P., 1997. Upper mantle velocity structure beneath Italy from direct and secondary P-wave teleseismic tomography. Ann. Geofis. XL, 175–194.

Cioni, R., 2000. Volatile content and degassing processes in the AD 79 magma chamber at Vesuvius (Italy). Contrib. Mineral. Petrol. 140, 40–54.

Cioni, R., Civetta, L., Marianelli, P., Metrich, N., Santacroce, R., Sbrana, A., 1995. Compositional layering and syn-eruptive mixing of a periodically refilled shallow magma chamber: the AD 79 Plinian eruption of Vesuvius. J. Petrol. 36, 739–776.

Civetta, L., Santacroce, R., 1992. Steady state magma supply in the last 3400 years of Vesuvius activity. Acta Vulcanol. 2, 147–159.

Civetta, L., Galati, R., Santacroce, R., 1991. Magma mixing and convective compositional layering within the Vesuvius magma chamber. Bull. Volcanol. 53, 287–300.

Civetta, L., D'Antonio, M., De Lorenzo, S., Di Renzo, V., Gasparini, P., 2004. Thermal and geochemical constraints on the deep magmatic structure of Mt Vesuvius. J. Volcanol. Geotherm. Res. 133, 1–12.

Connor, B.C., Hill, E.B., Winfrey, B., Franklin, M.N., La Femina, C.P., 2001. Estimation of volcanic hazards from tephra fallout. Nat. Hazards Rev., 33–42 (February).

Corrado, G., Rapolla, A., 1981. The gravity field of Italy: analysis of its spectral composition and delineation of a three-dimensional crustal model for central-southern Italy. Boll. Geofis. Teor. Appl. XXIII (89), 17–29.

De Astis, G., Pappalardo, L., Piochi, M., 2004. Procida Volcanic History: new insights in the evolution of the Phlegraean Volcanic District (Campania region, Italy). Bull. Volcanol. 66, 622–641. doi:10.1007/s00445-004-0345-y.

De Gori, P., Cimini, G.B., Chiarabba, C., De Natale, G., Troise, C., Deschamps, A., 2001. Teleseismic tomography of the Campanian volcanic area and surrounding Apenninic belt. J. Volcanol. Geotherm. Res. 109 (1–3), 52–75.

De Natale, G., Capuano, P., Troise, C., Zollo, A., 1998. Seismicity at Somma–Vesuvius and its implications for the 3-D tomography of volcano. J. Volcanol. Geotherm. Res. 82, 175–197.

De Natale, G., Petrazzuoli, S.M., Troise, C., Pingue, F., Capuano, P., 2000. Internal stress field at Mt. Vesuvius: a model for the generation of background seismicity at a central volcano. J. Geophys. Res. 105 (B7), 16207–16214.

De Natale, G., Troise, C., Pingue, F., De Gori, P., Chiarabba, C., 2001. Structure and dynamics of the Somma–Vesuvius volcanic complex. Mineral. Petrol. 73 (1–3), 5–22.

De Natale, G., Chiarabba, C., Troise, C., Trigila, R., Dolfi, D., Kissling, E., 2004a. Seismicity and 3D sub-structure at Somma–Vesuvius volcano: evidence for magma quenching due to H_2O exolution? Earth Planet. Sci. Lett. 221, 181–196.

De Natale, G., Kuznetzov, I., Kronrod, T., Peresan, A., Saraò, A., Troise, C., Panza, G., 2004b. Three decades of seismic activity at Mt. Vesuvius: 1972–2000. Pure Appl. Geophys. 161, 123–144.

De Vivo, B., Scandone, R., Trigila, R. (Eds.), Mount Vesuvius, Journ. Geotherm. Res., vol. 58, no.1/4.

Del Moro, A., Fulignati, P., Marianelli, P., Sbrana, A., 2001. Magma contamination by direct wall rock interaction: constraints from xenoliths from the walls of a carbonate-hosted magma chamber (Vesuvius 1944 eruption). J. Volcanol. Geotherm. Res. 112, 15–24.

Del Pezzo, E., Bianco, F., Saccorotti, G., 2004. Seismic source dynamics at Vesuvius volcano, Italy. J. Volcanol. Geotherm. Res. 133, 23–29.

Di Maio, R., Mauriello, P., Patella, D., Petrillo, Z., Piscitelli, S., Siniscalchi, A., 1998. Electric and electromagnetic outline of the Mount Somma–Vesuvius structural setting. J. Volcanol. Geotherm. Res. 82 (1–4), 219–238.

Di Stefano, R., Chiarabba, C., 2002. Active source tomography at Mt. Vesuvius: constraints for the magmatic system. J. Geophys. Res. 107 (B11), 2278–2292.

Di Stefano, R., Chiarabba, C., Lucente, F.P., Amato, A., 1999. Crustal and uppermost mantle structure in Italy from the inversion of P-wave travel times: geodynamics implications. Geophys. J. Int. 139, 483–498.

Doglioni, C., Mongelli, F., Pieri, P., 1994. The Puglia uplift (SE Italy): an anomaly in the foreland of the Apenninic subduction due to buckling of a tick continental lithosphere. Tectonics 13, 1309–1321.

Eberhart-Phillips, D., Reyners, M., 1997. Continental subduction and three-dimensional crustal structure: the northern South Island, New Zealand. J. Geophys. Res. 102, 11843–11861.

Fedi, M., Florio, G., Rapolla, A., 1998. 2.5D modelling of Somma–Vesuvius structure by aeromagnetic data. J. Volcanol. Geotherm. Res. 82 (1–4), 239–247.

Ferrucci, F., Gaudiosi, G., Pino, N.A., Luongo, G., Hirn, A., Mirabile, L., 1989. Seismic detection of a major Moho upheaval beneath the Campania volcanic area (Naples, Southern Italy). Geophys. Res. Lett. 16, 1317–1320.

Ferrucci, F., Hirn, A., De Natale, G., Virieux, J., e Mirabile, L., 1992. P–SV conversions at a shallow boundary beneath Campi Flegrei caldera (Italy): evidence for the magma chamber boundaries. J. Geophys. Res. 97 (B11), 15351–15359.

Friedlander, S.K., 2000. Smoke, Dust and Haze: Fundamentals of Aerosol Behaviour. Wiley, New York.

Fulignati, P., Marianelli, P., Sbrana, A., 1998. New insights on the thermometamorphic–metasomatic magma chamber shell of the 1944 eruption of Vesuvius. Acta Vulcanol. 10 (1), 47–54.

Fulignati, P., Marianelli, P., Metrich, N., Santacroce, R., Sbrana, A., 2004. Towards a reconstruction of the magmatic feeding system of the 1944 eruption of Mt Vesuvius. J. Volcanol. Geotherm. Res. 113, 13–22.

Gardner, C.A., Cashman, K.V., Neal, C.A., 1998. Tephra-fall deposits from the 1992 eruption of Crater Peak, Alaska: implications of clast textures for eruptive processes. Bull. Volcanol. 59, 537–555.

Gasparini, P., Tomoves Working Group, 1998. Looking inside Mt. Vesuvius. EOS, Trans., AGU 79 (229,230,232).

Hammer, J.E., Cashman, K.V., Hoblitt, R.P., 1999. Degassing and microlite crystallization during pre-climatic events of the 1991 eruption of Mt. Pinatubo, Philippines. Bull. Volcanol. 60, 355–380.

Hill, D.P., 1992. Temperatures at the base of the seismogenetic crust beneath Long Valley Caldera, California, and Phlegrean Fields caldera, Italy. In: Gasparini, P., Scarpa, R., Aki, K. (Eds.), Volcanic Seismology. Springer Verlag, pp. 432–461.

Joupart, Tait, 1990. Dynamics of eruptive phenomena. Rev. Mineral. Geochem. 24, 213–238.

Klein, F.W., 1989. User's Guide to HYPOINVERSE, A program for VAX Computers to Solve Earthquake Locations and Magnitudes, USGS Open-File Rept., pp. 89–314.

Lanari, R., De Natale, G., Berardino, P., Sansosti, E., Ricciardi, R., Borgstrom, S., Capuano, P., Pingue, F., Troise, C., 2002. Evidence for a peculiar style of ground deformation inferred at Vesuvius volcano. Geophys. Res. Lett. 29 (9), 10.1029.

Landi, P., Bertagnini, A., Rosi, M., 1999. Chemical zoning and crystallization mechanisms in the magma chamber of the Pomici di Base Plinian eruption of Somma–Vesuvius (Italy). Contrib. Mineral. Petrol. 135, 179–197.

Lima, A., Danyushevsky, L.V., De Vivo, B., Fedele, L., 2003. A model for the evolution of the Mt. Somma–Vesuvius magmatic system based on fluid and melt inclusion investigations, In Melt inclusions in volcanic systems: methods, applications and problems. In: De Vivo, B., Bodnar, R.J. (Eds.), Development in Volcanology. Elsevier press, p. 272.

Lirer, L., Munno, R., Petrosino, P., Vinci, A., 1993. Tephrostratigraphy of the AD 79 pyroclastic deposits in peri-volcanic areas of Mt. Vesuvio, Italy. J. Volcanol. Geotherm. Res. 58, 133–149.

Lomax, A., Zollo, A., Capuano, P., Virieux, J., 2001. Precise, absolute earthquake location under Somma–Vesuvius volcano using a new 3D velocity model. Geophys. J. Int. 146 (2), 313–331.

Lucente, F.P., Chiarabba, C., Cimini, G.B., Giardini, D., 1999. Tomographic constraints on the geodynamic evolution of the Italian region. J. Geophys. Res. 104, 20307–20327.

Marianelli, P., Métrich, N., Sbrana, A., 1999. Shallow and deep reservoirs involved in magma supply of the 1944 eruption of Vesuvius. Bull. Volcanol. 61, 48–63.

Marsh, B.D., 1988. Crystal size distribution (CSD) in rocks and kinetics and dynamics of crystallization: I. Theory. Contrib. Mineral. Petrol. 99, 277–291.

Mastrolorenzo, G., Munno, R., Rolandi, G., 1993. Vesuvius 1906: a case study of a paroxysmal eruption and its relation to eruption cycles. J. Volcanol. Geotherm. Res. 58, 217–237.

Mastrolorenzo, G., Brachi, L., Canzanella, A., 2001. Vesicularity of various types of pyroclastic deposits of Campi Flegrei volcanic field: evidence of analogies in magma rise and vesiculation mechanisms. J. Volcanol. Geotherm. Res. 109, 41–53.

Mastrolorenzo, G., Palladino, D., Vecchio, G., Taddeucci, J., 2002. The 472 AD Pollena eruption of Somma–Vesuvius (Italy) and its environmental impact at the end of the Roman Empire. J. Volcanol. Geotherm. Res. 113, 19–36.

McEwen, A.S., Malin, M.C., 1989. Dynamics of Mount St. Helens' 1980 pyroclastic flow, rockslide–avalanche, lahars, and blast. J. Volcanol. Geotherm. Res. 37, 205–231.

McNutt, S.R., 1996. Seismic monitoring and eruption forecasting of volcanoes: a review of the state-of-the-art and case histories. In: Scarpa, R., Tilling, R.I. (Eds.), Monitoring and Mitigation of Volcano Hazard. Springer Verlag, pp. 99–146.

Menke, W., 1984. Geophysical Data Analysis: Discrete Inverse Theory. Academic Press. 260 pp.

Meredith, P.G., Main, I.G., Jones, C., 1990. Temporal variations in seismicity during quasi-static and dynamic rock failure. Tectonophysics 175, 249–268.

Middleton, G.V., Southard, J.B., 1978. Mechanism of Sediment Movement. Soc. Econ. Paleontol. Mineral., Eastern Sec., Short Course Lecture Notes. 254 pp.

Mostardini, P., Merlini, S., 1986. Appennino centro-meridionale: sezioni geologiche e proposta di modello strutturale. Mem. Soc. Geol. Ital. 35, 177–202.

Natale, M., Nunziata, C., Panza, G.F., in press. Average shear wave velocity models of the crustal structure at Mt. Vesuvius, Phys. Earth Planet. Int.

Panza, G.F., Romanelli, F., 2001. Beno Gutenberg contribution to seismic hazard assessment and recent progress in the European–Mediterranean region. Earth Sci. Rev. 55, 165–180.

Panza, G.F., Pontevivo, A., Chimera, G., Raykova, R., Aoudia, A., 2003. The Lithosphere–Asthenosphere: Italy and surroundings. Episodes 26, 169–174.

Pappalardo, L., Piochi, M., D'Antonio, M., Civetta, L., Petrini, R., 2002. Evidence for multi-stage magmatic evolution during the past 60 ka at Campi Flegrei (Italy) deduced from Sr, Nd and Pb isotope data. J. Petrol. 43 (7), 1415–1434.

Pappalardo, L., Piochi, M., Mastrolorenzo, G., 2004. The 3800 yr BP-1944 AD magma plumbing system of Somma–Vesuvius: constraints on its behaviour and present state through a review of isotope data. In: De Natale, L., De Vivo (Eds.), Ann. Geophys., special volume.

Patacca, E., Scandone, P., 1989. Post-Tortonian mountain building in the Apennines. The role of the passive sinking of a relic lithospheric slab, in the Lithosphere in Italy, Advances in Earth Science Research (eds. A. Boriani et al.), CNR, Accademia Nazionale dei Lincei, pp. 157–176.

Peccerillo, A., 2001. Geochemical similarities between the Vesuvius, Phlegraean Fields and Stromboli Volcanoes: petrogenetic, geodynamic and volcanological implications. Mineral. Petrol. 73, 93–105.

Perla, R.I., 1980. Avalanche release, motion and impact. In: Colbeck, S.C. (Ed.), Dynamics of Snow and Ice Avalanches. Academic press, New York, pp. 397–462.

Piochi, M., Pappalardo, L., De Astis, G., 2004. Geochemical and isotopical variation within the Campanian Comagmatic Province: implications on magma source composition. In: De Natale, G., De Vivo (Eds.), Ann. Geophys., Volcanic Systems, Geochemical and Geophysical Monitoring. Melt Inclusions: Methods, Applications and Problems. Ann. Geophys, vol. 74 (4), pp. 1485–1499.

Presti, D., Troise, C., De Natale, G., 2004. Probabilistic location of seismic sequences in heterogeneous media. Bull. Seismol. Soc. Am. 94 (6), 2239–2263.

Rolandi, G., Barrella, A.M., Borrelli, A., 1993. The 1631 eruption of Vesuvius. J. Volcanol. Geotherm. Res. 58, 183–201.

Rosi, M., Principe, C., Vecci, R., 1993. The 1631 Vesuvius eruption. Reconstruction based on historical and stratigraphical data. J. Volcanol. Geotherm. Res. 58, 151–182.

Rossano, S., Mastrolorenzo, G., De Natale, G., Pingue, F., 1996. Computer simulation of pyroclastic flow movement: an inverse approach. Geophys. Res. Lett. 23, 3779–3782.

Rossano, S., Mastrolorenzo, G., De Natale, G., 1998. Computer simulation of pyroclastic flow movement on Somma–Vesuvius volcano. J. Volcanol. Geotherm. Res. 82, 113–137.

Rossano, S., Mastrolorenzo, G., De Natale, G., 2004. Numerical simulation of pyroclastic density currents on Campi Flegrei topography: a tool for statistical hazard estimation. J. Volcanol. Geotherm. Res. 132, 1–14.

Russo, G., Giberti, G., Sartoris, G., 1997. Numerical modeling of surface deformation and mechanical stability of Vesuvius Volcano, Italy. J. Geophys. Res. 102, 24785–24800.

Santacroce, R., 1987. Somma–Vesuvius. CNR Quaderni de "La Ricerca Scientifica", p. 251.

Santacroce, R., Bertagnini, A., Civetta, L., Landi, P., Sbrana, A., 1993. Eruptive dynamics and petrogenetic processes in a very shallow magma reservoir: the 1906 eruption of Vesuvius. J. Petrol. 34, 383–425.

Scandone, R., Iannone, F., Mastrolorenzo, G., 1986. Stima dei parametri eruttivi dell'eruzione del 1944, Boll. Gruppo Nazionale Vulcanologia.

Selvaggi, G., Amato, A., 1992. Intermediate-depth earthquake in northern Apennines (Italy): evidence for a still active subduction? Geophys. Res. Lett. 19, 2127–2130.

Sigurdsson, H., Carey, S., Cornell, W., Pescatore, T., 1985. The eruption of Vesuvius in AD 79. Nation. Geogr. Res. 1 (3), 332–387.

Suzuki, T., 1983. A theoretical model for the dispersion of tephra. In: Shimozuru, D., Yokiyama, I. (Eds.), Arc Volcanism: Physics and Tectonics. Terra Scientific Publishing Company, Tokyo, pp. 95–113.

Terada, T., 1929. On the form of volcanoes, Bull. Earthq. Res. Inst., Univ. Tokyo, 7, 207–221.U.S. Standard Atmosphere, 1976, U.S. Government Printing Office, Washington, D.C., 1976.

Vilardo, G., De Natale, G., Milano, G., Coppa, U., 1996. The seismicity of Mt. Vesuvius. Tectonophysics 261, 127–138.

Villemant, B., Trigila, R., De Vivo, 1993. Geochemistry of Vesuvius volcanics during 1631–1944 period. J. Volcanol. Geotherm. Res. 58, 291–313.

Woods, A.W., 1988. The fluid dynamics and thermodynamics of eruption columns. Bull. Volcanol. 50, 169–193.

Zollo, A., Gasparini, P., Biella, G., De Franco, R., Buonocore, B., Mirabile, L., De Natale, G., Milano, G., Pingue, F., Vilardo, G., Bruno, P.P., De Matteis, R., Le Meur, H., Iannaccone, G., Deschamps, A., Virieux, J., Nardi, A., Frepoli, A., Hunstad, I., Guerra, I., 1996. 2D seismic tomography of Somma–Vesuvius: description of the experiment and preliminary results. Ann. Geofis. 9, 471–486.

Zollo, A., Gasparini, P., Virieux, J., Le Meur, H., De Natale, G., Biella, G., Boschi, E., Capuano, P., De Franco, R., Dell'Aversana, P., De Matteis, R., Guerra, I., Iannaccone, G., Mirabile, L., Vilardo, G., 1996. Seismic evidence for a low-velocity zone in the upper crust beneath Mount Vesuvius. Science 274, 592–594.